PHASE RELATIONS AND CERTAIN MAGNETIC CHARACTERISTICS
OF
SOME RE-Co-Fe ALLOYS

By

M. V. SATYANARAYANA

MSP
1977
M
SAT
PHA

TH
MSP/1977/M
Sa84p

INTERDISCIPLINARY PROGRAMME IN MATERIALS SCIENCE

INDIAN INSTITUTE OF TECHNOLOGY KANPUR

JANUARY, 1977

A 51149

PHASE RELATIONS AND CERTAIN MAGNETIC CHARACTERISTICS OF SOME RE-Co-Fe ALLOYS

A Thesis Submitted
In Partial Fulfilment of the Requirements
for the Degree of
MASTER OF TECHNOLOGY

By
M. V. SATYANARAYANA

to the

INTERDISCIPLINARY PROGRAMME IN MATERIALS SCIENCE
INDIAN INSTITUTE OF TECHNOLOGY KANPUR
JANUARY, 1977

MSP-1977-M-SAT-PHA

I.I.T. KANPUR
CENTRAL LIBRARY
Acc. No. A 51149

11 th

CERTIFICATE

This is to certify that this work on 'Phase Relations and Certain Magnetic Characteristics of some RE-Co-Fe Alloys' has been carried out under my supervision and it has not been submitted elsewhere for a degree.

Dr. K.P. Gupta
Professor
Department of Metallurgical Engg.
Indian Institute of Technology.
KANPUR

POST GR [illegible]
This thes [illegible]
fo [illegible]
M [illegible]
[illegible] the
Feb 22, 1977

ACKNOWLEDGEMENT

I wish to express my deep sense of gratitude to Professor K.P. Gupta for his excellent guidance and help throughout this investigation. It has been an invaluable experience to work under his supervision.

I am highly grateful to Professor E.C. Subbarao for his kind encouragement and advice from time to time. It is his keen interest in my welfare that made this work to be completed so successfully.

I am thankful to all the members of the project - Dr. A.K. Majumdar, Dr. H.O. Gupta, Dr. S.N. Kaul, Mr. G. Sarkar, Mr. E.M.T. Velu and Mr. S.S. Sehgal. I am especially thankful to Mr. R.C. Mittal for his assistance throughout this investigation.

I am grateful to Mr. V.P. Gupta for his help in the fabrication work and in preparing the figures. I am thankful to Mr. B. Sharma, Mr. R.K. Prasad and Mr. O.P. Malaviya for their help in the fabrication of ceramic crucibles etc., to Mr. N.R. Yadav for his help in the x-ray work and to Mr. K.P. Mukherjee for his help in the metallography work.

This project was supported by the Electronics Commission of India and I am grateful to them.

Finally, I wish to thank Mr. R.S. Misra for typing the manuscript and Mr. Vishwanath Singh for his general help.

M.V. SATYANARAYANA

TABLE OF CONTENTS

LIST OF TABLES

LIST OF FIGURES

SYNOPSIS

CHAPTER I INTRODUCTION 1

I.1 Literature Review 5

I.2 Statement of Problem 22

CHAPTER II THERMAL ANALYSIS APPARATUS 25

II.1 Design and Description of Apparatus 25

II.2 Testing and Calibration 32

CHAPTER III EXPERIMENTAL PROCEDURE 39

III.1 Phase Equilibria in RE-Co-Fe System 39

III.2 Thermal Analysis 48

III.3 Curie Temperature Measurement 50

III.4 Magnetic Easy Axis Determination 52

CHAPTER IV RESULTS AND DISCUSSION 54

IV.1 Phase Equilibria 54

IV.2 Easy Axis of Magnetization 75

IV.3 Curie Temperature 76

IV.4 Thermal Analysis 80

CONCLUSIONS 84

SUGGESTIONS 86

REFERENCES 88

APPENDIX I 92

LIST OF TABLES

Table No.

I.1 Magnetic properties of some selected permanent magnetic materials. 3

I.2 Physical and magnetic properties of rare earth elements. 6

I.3 Lattice constants and structural characteristics of some important RE-Co phases. 10

I.4 Magnetic properties of $RECo_5$ compounds 14

II.1 Thermocouple calibration data 38

IV.1 Phase analysis of the RE-Co-Fe System 55

IV.2 Chemical analysis of several RE-Co-Fe alloys 57

IV.3 X-ray diffraction pattern of the A-phase 65

IV.4 X-ray diffraction pattern of the S phase 68

IV.5 X-ray diffraction pattern of the A_2B_7-type phase 71

IV.6 Lattice parameters of S and A phases in the RE-Co-Fe System 73

IV.7 Curie temperatures of RE-Co-Fe alloys 79

LIST OF FIGURES

FIGURE No.

I.1 Phase diagrams of Sm-Co, Ce-Co, La-Co and Ce-Fe Systems
I.2 Phase diagram of the Pr-Co system
I.3 Phase diagram of the Nd-Co system
I.4 $CaCu_5$ type structure: (a) hexagonal unit cell; (b) rhombohedral unit cell
I.5 Mode of formation of hexagonal and rhombohedral RE_xCo_y alloys out of the $RECo_5$ structure: (a) RE_2Co_7 alloy; (b) RE_2Co_{17} alloy.
I.6 Saturation Induction of several rare earth (T)-cobalt (Co) phases.
I.7 Curie temperatures of several rare earth (T)-cobalt (Co) phases.
I.8 Values of $4\pi M_s$, T_c and H_A for the $Sm_2(Co,Fe)_{17}$ alloys
I.9 Magnetic symmetry of the $RE_2(Co_{1-x}Fe_x)_{17}$ phases
II.1 Thermal analysis apparatus
II.2 Block diagram representing thermal analysis set up
II.3 Furnace power supply circuit
II.4 Thermocouple output measurement circuit
II.5 Typical cooling curves: (a) Germanium; (b) Gold; (c) Fe-Si eutectic
II.6 Thermocouple Calibration Curve
III.1 Block diagram representing gas purification system
IV.1 Isothermal section of the RE-Co-Fe system at 900°C
IV.2 Microstructure of alloy 14
IV.3 Microstructure of alloy 15
IV.4 Microstructure of alloy 31
IV.5 Microstructure of alloy 51
IV.6 Microstructure of alloy 52
IV.7 Microstructure of alloy 34
IV.8 Microstructure of alloy 42
IV.9 X-ray diffractometer relative intensity data of of RE_2Co_{17}, A and S phases.

IV.10 Hexagonal Th_2Ni_{17} structure

IV.11 Schematic representation of stacking of blocks in Th_2Zn_{17} structure.

IV.12 Schematic representation of Th_2Zn_{17}-type and Th_2Ni_{17} - type structures

IV.13 Lattice parameters of RE-Co-Fe phases (a) A phase; (b) S phase

IV.14 Curie temperature plot for RE_2Co_7 phase

IV.15 Curie temperature plot for A phase

IV.16 Curie temperature plot for alloy 30

IV.17 Curie temperature plot for S phase

IV.18 Curie temperatures of RE-Co-Fe phases

SYNOPSIS

Rare Earth - Cobalt intermetallic compounds represent a new class of materials with excellent permanent magnet properties. But, the high raw material costs restrict the application of these magnets to limited fields. The use of relatively cheap raw materials, mischmetal and iron to replace the individual rare earth elements and part of cobalt is very helpful from an economic point of view if a compromise with the magnetic properties can be made. With these points in view, a study of the MM-Co-Fe system has been taken up in the present investigation.

To establish the different phases that exist in the MM-Co-Fe system, the phase equilibria work was carried out. Alloys of different compositions were melted, under purified argon atmosphere, in a non-consumable tungsten electrode water-cooled copper hearth arc melting furnace. A gas purification system was fabricated and used for purifying the argon gas. The as cast alloys were sealed in evacuated quartz tubes (20×10^{-3} mm Hg) and annealed at $900^{\circ}C$ for 4 days. The annealed alloys were used for metallographic and x-ray diffraction analysis. Nital etching reagent was found to be suitable for revealing the microstructures of most of the alloys. A diffractometer and a Debye-Scherrer Camera were used for obtaining the x-ray diffraction patterns of the RE-Co-Fe alloys. Besides the A_2B_7 type phase, two new phases, A phase and S phase, were found to exist in the investigated portion of the RE-Co-Fe system. The A_2B_7 phase was found to deviate from the hypothetical A_2B_7 quasi-binary line. The A phase was found to extend along the same direction as the A_2B_7 phase. The S phase was found to extend parallel to the quasi-binary A_2B_{17} line. The A and S phases appeared to have structures. similar to that of the RE_2Co_{17} phase. The lattice parameters of the A phase alloys were found to be insensitive to the change in Fe content whereas those of the S phase were found to increase with Fe content. These lattice parameter variations could not be explained on the basis of the available data.

In order to get a first hand information of favourable magnetic characteristics of the RE-Co-Fe alloys, the Curie temperatures and the easy axis of magnetization were determined for a few important alloy compositions. The Curie temperatures (T_c) were determined by the induction method. The T_c values of different phases appear to vary smoothly with Fe content. Among the investigated alloys, the Curie temperatures of the

S phase alloys are the highest and those of the A phase alloys are the lowest. The easy axis of magnetization of the S phase was determined in the same way as the fibre axis determination. Magnetically aligned needles were prepared from powdered alloys and the x-ray pattern was obtained using a Weissenberg Camera. Etching of the alloy powder was found to produce good streaky pattern as expected from a well aligned specimen. The magnetic easy axis for the S phase was found to be along the c-axis. On the basis of the available data, the S phase appears to be the most promising for permanent magnet development.

For determining the melting points of the RE-Co-Fe alloys, an already available system was converted to a thermal analysis apparatus. Since a heater element of suitable gauge was not available, a two-layer furnace with a room temperature resistance of about 3 ohms was fabricated using available Mo wire. The furnace assembly was calibrated using standard samples of known melting points. Attempts to carry out thermal analysis of the RE-Co-Fe alloys were not successful because the furnace failed during thermal analysis of RE-Co-Fe alloys. However, several important observations regarding the operation of the apparatus and the melting points of the $RECo_5$ and RE_2Co_{17} phases have been made. The melting points of the ternary A_2B_{17} type phase near the RE-Co binary phase appears to be above 1400°C, well above that of the binary compound. The melting point of the $RECo_5$ type phase appears to be below 1250°C.

CHAPTER I

INTRODUCTION

Permanent magnets play an important and essential part in many devices where an electromagnet cannot be used. Materials for these magnets have been developed from the high carbon chromium steels to alnicos in the present century (1). But, more recently, another new class of magnets based on rare earth-transition metal compounds, with outstanding permanent magnet properties, have come into existence. The sequence of events which led to the development of these materials for permanent magnet applications can be listed as follows: the discovery, in 1935 by Urbain, Weiss and Trombe (2), of the ferromagnetism of Gd, the report on the saturation magnetization of Gd-Fe and Gd-Co alloys in 1959 by Nesbitt et al. (3), the notable work of Hubbard, Adams and Gilfrich in 1960 on the permanent magnet properties of $GdCo_5$ alloy (4), and the discovery of an extremely high magnetocrystalline anisotropy for YCo_5 in 1966 by Hoffer and Strnat (5). The slow progress in this field upto 1966 can be traced to the unavailability of pure rare earth metals in the early periods, their high costs, the lack of understanding of the parameters that influence the magnetic properties and not recognizing $GdCo_5$ as one of a family of compounds. The discovery of Hoffer and Strnat, however, was followed by extensive studies to determine the permanent magnet properties of the family of rare earth-transition metal compounds. These compounds, particularly the light rare earth (at nos. 57-63) - cobalt compounds are reported to have high remanent magnetization and coercivity. The useful magnetic properties of $SmCo_5$ and (Sm, Pr) Co_5 alloys are compared with those of the conventional permanent magnetic materials in Table I.1.

Most of todays rare earth-transition metal permanent magnets are based on $SmCo_5$. This is because of the fact that $SmCo_5$ magnets with excellent magnetic properties can be fabricated relatively easily. Nevertheless it has become increasingly apparent that not all the properties of a permanent magnet are equally important in a given application. For example, in applications with a relatively narrow air gap where the magnet operates at a high load line $- B/\mu_0 H$ (like in motors and generators), an extremely high resistance to demagnetization is not necessary. As a result, in such applications, the potential of the $SmCo_5$ magnets is not completely utilized. Also, the relatively high price of samarium restricts the application of $SmCo_5$ magnets to fields where the costs are determined by production processes rather than

TABLE I.1

Magnetic Properties of Some Selected Permanent Magnetic Materials (1)

Material	Typical Magnetic Properties		
	Remanent Induction Br, kG	Coercive Force H_c, Oe	Maximum Energy Product $(BH)_{max}$, MGOe
3.5 percent Cr steel	9.5	66	0.29
40 percent Co steel	10.0	242	1.03
Alnico 1	6.6	540	1.40
Alnico 5	12.0	720	5.0
Alnico 5 DG	13.3	685	6.5
Alnico 8	7.1	2000	5.5
Alnico 9	10.4	1600	8.5
Cunife 1	5.7	590	1.85
Cunico 1	3.4	710	0.85
Remalloy	10.5	250	1.1
Vicalloy 2	10.0	450	3.0
Platinum-Cobalt	6.45	4300	9.5
Ceramic			
i) isotropic barium ferrite	2.25	1850	1.15
ii) anisotropic barium ferrite	3.95	2400	3.5
iii) anisotropic strontium ferrite	3.425	3300	2.9
$SmCo_5$ [x]	9.0	9000	20.0
$(Sm,Pr)Co_5$ [x]	9.9	6800	23.0

[x] values for these materials are quoted from references (6) and (7) respectively.

by those of the raw material. The wider scope of the application of rare earth-cobalt magnets requires the material costs to be lowered while new types of magnets with specific application - oriented properties are developed. Magnets of somewhat inferior magnetic qualities than the $SmCo_5$ magnets may thus be useful for various applications. The rare earth elements occur together in the ores and at present it is the cost of separation that makes the individual metals so expensive. Since the highest magnetic qualities are not always required, efforts are underway to replace samarium by the cheaper mixture of rare earths, the mischmetal (MM). This is of particular importance to India where vast deposits of rare earths (in Kerala sands) are available. The other component of the rare earth magnets, cobalt, is also expensive, particularly in India because it has to be imported. There are indications that partial iron substitution for cobalt improves the properties of cobalt rich rare earth-cobalt alloys to some extent (8). Hence, substitution of Co by iron in MM-Co magnets, at least in part, is expected to be a valuable contribution towards cost reduction. So, a thorough investigation of the MM-Co-Fe system was thought very essential and has been taken up in this investigation.

I.1 Literature Review:

The term 'Rare Earth' refers to the 4f-transition elements with atomic numbers between 57 (Lanthanum) and 71 (Lutetium). Yttrium (39) is also included in this group because of its close resemblance in properties to the rare earths. Gadolinium (64) for which the 4f shell is half filled divides the rare earths into light (less than half filled) and heavy (more than half filled) rare earths. For the light rare earths the orbital moment L and the spin moment S are antiparallel to each other so that the resultant magnetic moment has the magnitude $J : |L - S|$. On the other hand, for the heavy rare earths the orbital and spin moments are parallel and $J : |L + S|$. This behaviour has important implications for the total magnetic moment of the RE-Co compounds.

In their elemental form, the rare earths have very interesting magnetic properties. Some of their physical and magnetic properties are listed in Table I.2. As seen from the Table, some of the elements like Y, La or Lu have no permanent magnetic moment (in their usual valence state, +3) while others are magnetic. Due to strong crystal field effects, the ferromagnetic rare earths also exhibit extremely high magnetocrystalline anisotropy (9). The element dysprosium, for example, has the highest known saturation magnetization, 37,950 gauss, and the highest uniaxial anisotropy constant,

TABLE I.2

Physical and Magnetic Properties of Rare Earth Elements (9)

Element	Atomic no.	Metallic valence	Melting point, °C	Boilling point, °C	Free atom electronic configuration.	Magnetic moment/atom μ_B	Curie Temperature T_c, °C
Lanthanum	57	3	920	3454	$5d^1 6s^2$	0	None
Cerium	58	3,4	798	3257	$4f^1 5d^1 6s^2$	2.56	-
Praseodymium	59	3	931	3212	$4f^2 5d^1 6s^2$	3.62	None
Neodymium	60	3	1010	3127	$4f^3 5d^1 6s^2$	3.68	-
Promethium	61	3	1035	2700	$4f^4 5d^1 6s^2$	2.83	-
Samarium	62	3	1072	1778	$4f^5 5d^1 6s^2$	1.6	-
Europium	63	2	822	1597	$4f^6 5d^1 6s^2$	3.45	-165
Gadolinium	64	3	1311	3233	$4f^7 5d^1 6s^2$	7.94	+16
Terbium	65	3	1360	3041	$4f^8 5d^1 6s^2$	9.72	-36
Dysprosium	66	3	1409	2335	$4f^9 5d^1 6s^2$	10.6	-158
Holimium	67	3	1470	2720	$4f^{10} 5d^1 6s^2$	10.6	-253
Erbium	68	3	1522	2510	$4f^{11} 5d^1 6s^2$	9.6	-254
Thulium	69	3	1545	1727	$4f^{12} 5d^1 6s^2$	7.6	-
Ytterbium	70	2	824	1193	$4f^{13} 5d^1 6s^2$	4.5	None
Lutetium	71	3	1656	3315	$4f^{14} 5d^1 6s^2$	0	None
Yttrium	39	3	1523	3337	$4d^1 5s^2$	0	None

$K_1 = 10.9x10^8$ erg/cm^3 at 0°K. However, the magnetic order in the RE elements occurs only at low temperatures. The highest Curie temperature, among the rare earth elements, is that of Gd, 16°C (Table I.2). So, the pure rare earths are of no use for conventional magnetic applications. When a rare earth element and a 3d-transition metal are alloyed together, a number of intermediate phases form. These phases show ferro- , ferri- , or antiferromagnetic order at room temperature. Some of the ferromagnetic phases show Curie temperatures of several hundred degrees centigrade. In many of these phases the rare earth elements induce a high uniaxial crystal anisotropy which makes these substances interesting as hard magnetic materials (4).

The binary rare earth-transition metal systems have been studied for Mn, Fe, Co and Ni and magnetic properties of various phases formed have been determined to see which of the RE-transition metal phases are of practical importance. In the case of RE-Mn systems, the three phases, $REMn_{12}$, RE_6Mn_{23} and $REMn_2$ (No $REMn_5$ compound exists) have been found to exhibit either antiferromagnetic order or they are ferromagnetic with Curie temperatures too low to be of interest for permanent magnet use (10). In the case of RE-Ni systems, a variety of phases (RE_2Ni_7, $RENi_5$, RE_2Ni_{17} and other high RE phases) form but they have low Curie points (11).

The Ce-Fe diagram is shown in Fig. I.1. The other RE-Fe diagrams are reported to be having similar features (12). In the RE-Fe systems of Ce, Nd, Pr and Sm, recent investigations indicate that the $REFe_5$ phases, which were proposed by earlier investigators, do not exist. The only two phases that exist are $REFe_2$ and RE_2Fe_{17}. The RE_2Fe_{17} compounds are reported to have high saturation magnetization and uniaxial crystal symmetry, but they have low Curie points ($T_c < 180$) (13). T_c increases but the saturation magnetization drops. Thus, RE-transition metal compounds of Mn, Fe and Ni are not useful for permanent magnet applications. The RE-Co alloys, however, show magnetic characteristics (indicated later) which are highly attractive for permanent magnet applications. Also, there are indications that addition of Fe to some of the RE-Co compounds improves their magnetic characteristics (8). Thus, even though the RE-Fe alloys are not important for permanent magnet applications, RE-Co-Fe alloys may be quite promising.

The RE-Co systems are the most widely investigated ones among the RE-transition metal systems. Several of the binary RE-Co phase diagrams (for RE = Ce, La, Pr, Nd and Sm) are given in Figs. I.1 to I.3. As shown in the figures, all the binary RE-Co systems show the existence of RE_2Co_7, $RECo_5$ and RE_2Co_{17} phases and several high RE-Co phases. Those high

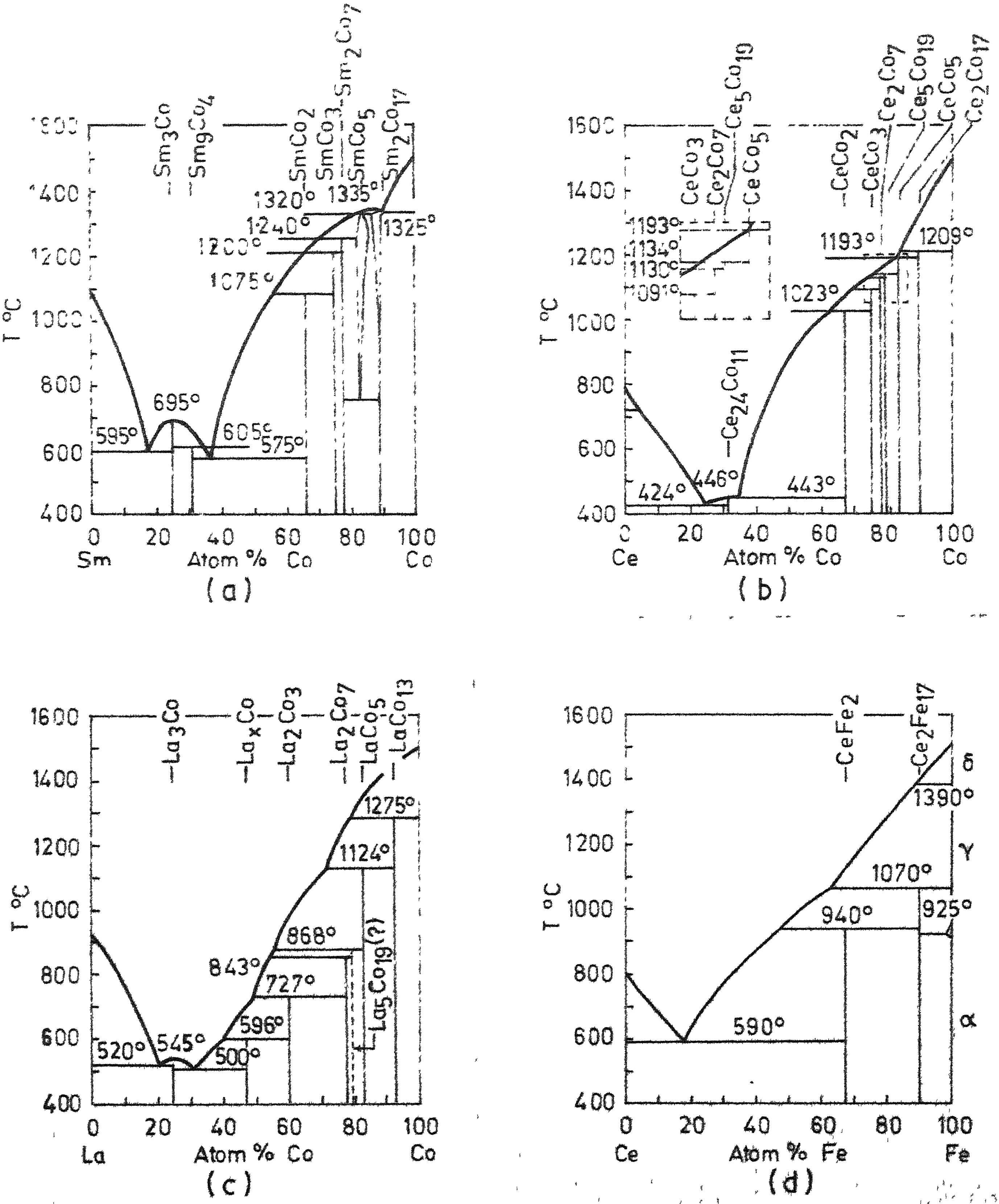

FIG. I.1. PHASE DIAGRAMS OF Sm-Co, Ce-Co, La-Co AND Ce-Fe SYSTEMS(14).

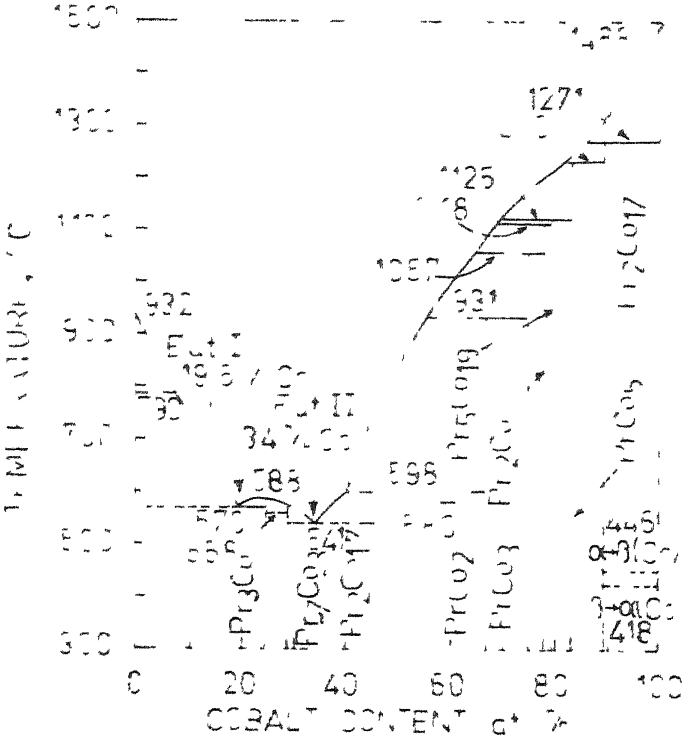

FIG I 2 PHASE DIAGRAM OF THE Pr-Co SYSTEM (15)

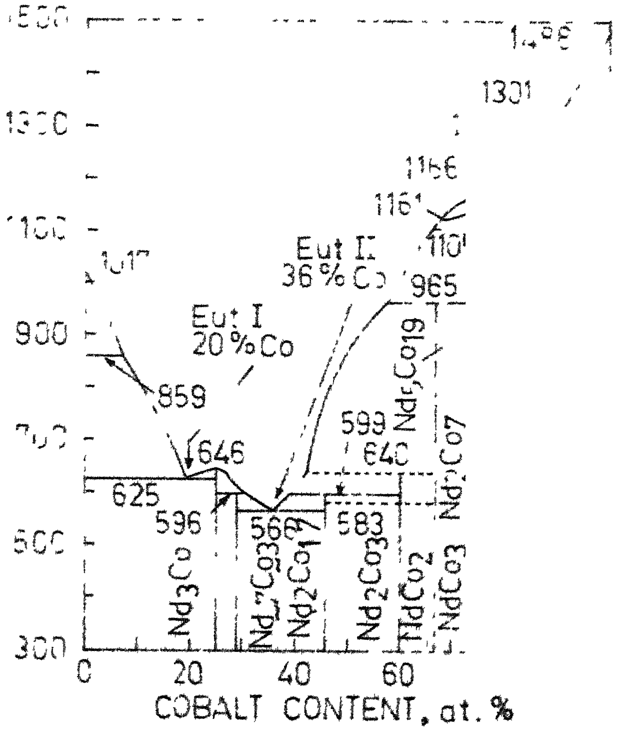

'HASE DIAGRAM OF THE Nd-Co SY

Co phases usually have a very narrow phase region. Only $RECo_5$ and RE_2Co_{17} compounds for Ce and Sm are reported to have an appreciable homogeneity region; the $RECo_5$ homogeneity region extends towards higher Co concentrations whereas the RE_2Co_{17} homogeneity region extends towards concentrations poorer in Co (16,17). Some of the $RECo_5$ compounds are reported to decompose eutectoidally into RE_2Co_7 and RE_2Co_{17} at low temperatures. For example, $SmCo_5$ decomposes at 750°C (13). Even though Buschow (18) has reported that the other $RECo_5$ phases also decompose at low temperatures, Ray (19) could not find any evidence of it. The RE_2Co_7 type compounds usually crystallize in the hexagonal Ce_2Ni_7 type structure with the exception that La_2Co_7 has both hexagonal and rhombohedral polymorphic structures (20). All the $RECo_5$ compounds have hexagonal $CaCu_5$ type structures whereas the RE_2Co_{17} compounds usually have rhombohedral Th_2Zn_{17} type structures. Sm_2Co_{17} and Ce_2Co_{17}, however, have both hexagonal (high temperature) and rhombohedral Th_2Zn_{17} type structures (12). Lattice constants and structural characteristics of some of the high Co containing phases, RE_2Co_7, $RECo_5$ and RE_2Co_{17} are listed in Table I.3.

TABLE I.3

Lattice Constants and Structural Characteristics of Some Important RE-Co Phases (15,16,20,56)

Compound	RE_2Co_7			$RECo_5$			RE_2Co_{17}		
Element	'a', A°	'c', A°	Structure type	'a', A°	'c', A°	Structure type	'a', A°	'c', A°	Structure type
Cerium	4.949	24.47	Hexagonal Ce_2Ni_7 type	4.928	4.015	Hexagonal $CaCu_5$ type	8.382	8.13	Hexagonal Th_2Ni_{17} type
							8.381	12.207	Rhombohedral Th_2Zn_{17} type
Lanthanum	5.101	24.511	Hexagonal Ce_2Ni_7 type	5.1	3.968	Hexagonal $CaCu_5$ type	11.344	-	Cubic $NaZn_{13}$ type^x
	5.11	36.69	Rhombohedral Gd_2Co_7 type						
Neodymium	5.063	24.45	Hexagonal Ce_2Ni_7 type	5.028	3.977	Hexagonal $CaCu_5$ type	8.426	12.245	Rhombohedral Th_2Zn_{17} type
Praseodymium	5.072	24.51	Hexagonal Ce_2Ni_7 type	5.032	3.992	Hexagonal $CaCu_5$ type	8.436	12.276	Rhombohedral Th_2Zn_{17} type
Samarium	5.041	24.327	Hexagonal Ce_2Ni_{17} type	5.002	3.964	Hexagonal $CaCu_5$ type	8.395	12.216	Rhombohedral Th_2Zn_{17} type (upto about 1200°C)
							8.36	8.515	Hexagonal Th_2Ni_{17} type

---

x [illegible] compound exists for La.

The hexagonal CaCu$_5$ structure of RE-Co alloys consists of an infinite stacking sequence of two different layers of atoms in the direction of the c-axis - a hexagonal arrangement of Co atoms followed by a mixed layer of RE and Co atoms as shown in Fig. I.4(a). The hexagonal cell of RECo$_5$ phase contains 3 rhombohedral unit cells (Fig. I.4(b)). The structures of the compounds in the range RECo$_2$ to RE$_2$Co$_{17}$ can be derived from the hexagonal RECo$_5$ structure (11,22). The mode of formation of hexagonal and rhombohedral structures of the RE$_2$Co$_7$ and RE$_2$Co$_{17}$ compounds from the RECo$_5$ structure is schematically shown in Figs. I.5(a) and (b).

Before discussing, the magnetic properties of the rare earth alloys, it will be of interest to recall which combination of properties qualifies a ferromagnetic substance for use as a permanent magnetic material. First of all, it must have a high saturation magnetization, M_s, at room temperature so that it can produce a remanent flux (B_R) of useful magnitude. The theoretical upper limit of the energy product (the maximum value of BXH in the second quadrant of the hysterisis loop), $(BH)_{max} = (2\pi M_s)^2$ in C.G.S. units, is also determined by M_s. Second, the Curie temperature, T_c, must be high. Finally, it is necessary that the intrinsic coercive force be sufficiently high, namely, ${}_{M}H_C > 2\pi M_s$, to allow a close approach to the theoretical energy product.

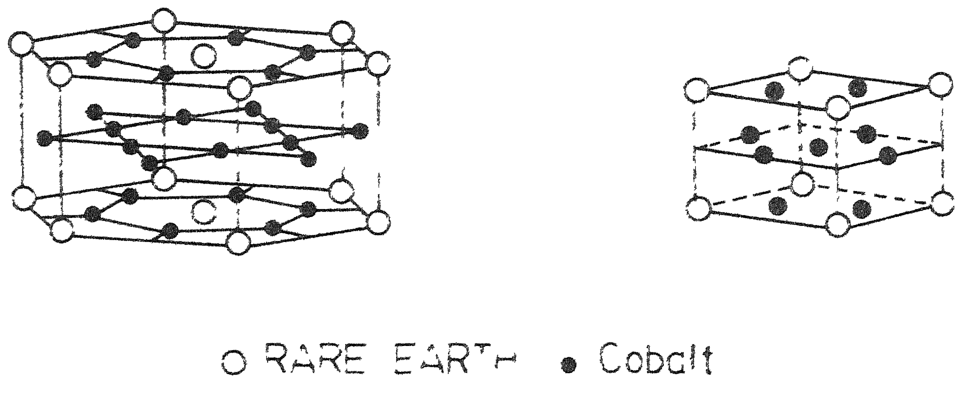

(a) (b)

FIG I 4 CaCu$_5$ TYPE STRUCTURE (a) HEXAGONAL UNIT CELL, (b) RHOMBOHEDRAL UNIT CELL (14)

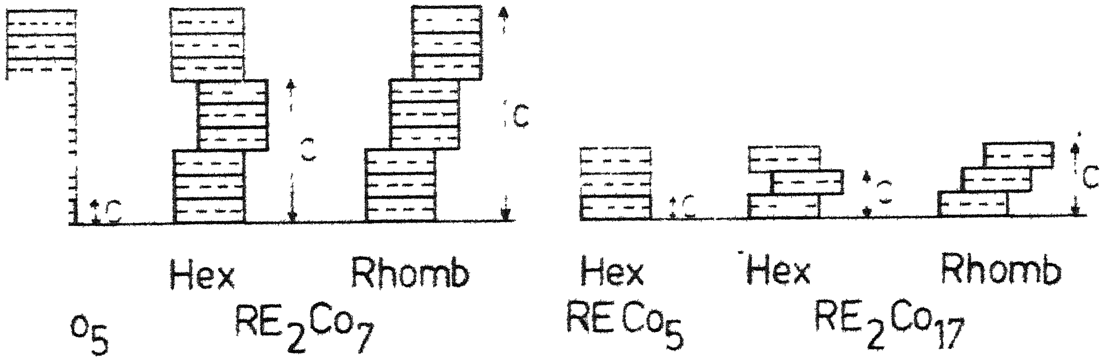

(a) (b)

. I 5 MODE OF FORMATION OF HEXAGONAL AND MBOHEDRAL RE$_x$Co$_y$ ALLOYS OUT OF THE RECo$_5$ UCTURE : (a) RE$_2$Co$_7$ ALLOY, (b) RE$_2$Co$_{17}$ ALLOY. (11)

According to the modern concept of permanent magnetism, such high coercive forces are only expected of a substance which has very large magnetocrystalline anisotropy (determined by the anisotropy field, H_A) and a single easy axis of magnetization.

The studies of Nassau, Cherry and Wallace (23) and Nesbitt et al (24) on the temperature dependence of magnetization for $RECo_5$ compounds revealed two different types of behaviour. For Y and the light rare earths, the magnetization increased with decreasing temperature whereas for Gd and the heavy rare earths, the magnetization decreased with decreasing temperature. These observations are consistent with the idea that the spin of the rare earth atoms always couples antiparallel with that of the cobalt atoms. Thus, in the light rare earth alloys, the total moment of the RE ($J = |L-S|$) adds to that of the cobalt leading to higher magnetization values. But, in the Gd and heavy rare earth alloys, the total rare earth moment ($J = |L+S|$) is antiparallel to that of cobalt leading to a two sub-lattice ferrimagnetism with the associated lowering of the total magnetization. Thus, the strongest magnetic moments are observed in alloys prepared with the largest rare earths or even with the non-magnetic Y. This is shown in Fig. I.6 in which the approximate values of the saturation induction,

$4\pi M_s$, for RE_2Co_{17}, $RECo_5$, RE_2Co_7 and RE_2Co_3 alloys are plotted as a function of the rare earth atoms. If the RE-Co magnets are to compete with the existing Alnico magnets, for example, the saturation induction at room temperature of the RE-Co compounds must reach at least 6000 Gauss. From Fig. I.6 it follows, then, that the convenient group of compounds is limited to the RE_2Co_{17} and $RECo_5$ compounds of Y and the light rare earths. Incidentally, these compounds also have high Curie temperatures as is shown in Fig. I.7.

The magnetic properties of the useful $RECo_5$ compounds are listed in Table I.4. As indicated in the table, the $RECo_5$ phases have very large (largest known) magnetocrystalline anisotropy values (as shown by the large anisotropy fields) and substantial values of saturation magnetization at room temperature. They also have the desirable easy c-axis magnetic symmetry. Permanent magnets based on these materials have now been made with previously unattainable coercivities and energy products. But, only in the case of $SmCo_5$ compound, energy product close to the theoretical limits has been achieved. As for example, Das (6) has reported a $(BH)_{max}$ value of 20 MGOe for liquid phase sintered $SmCo_5$ alloys which is very close to the theoretical value. In the case of the other $RECo_5$ compounds, further work has to be done to realize the theoretical values of $(BH)_{max}$.

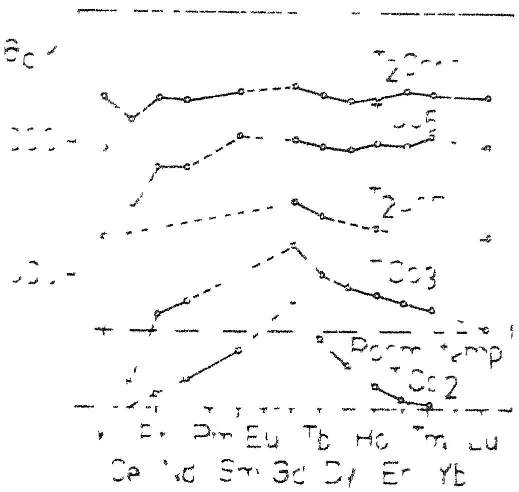

FIG I 7 CURIE TEMPERATURES OF SEVERAL RARE EARTH (T) COBALT (Co) PHASES (25)

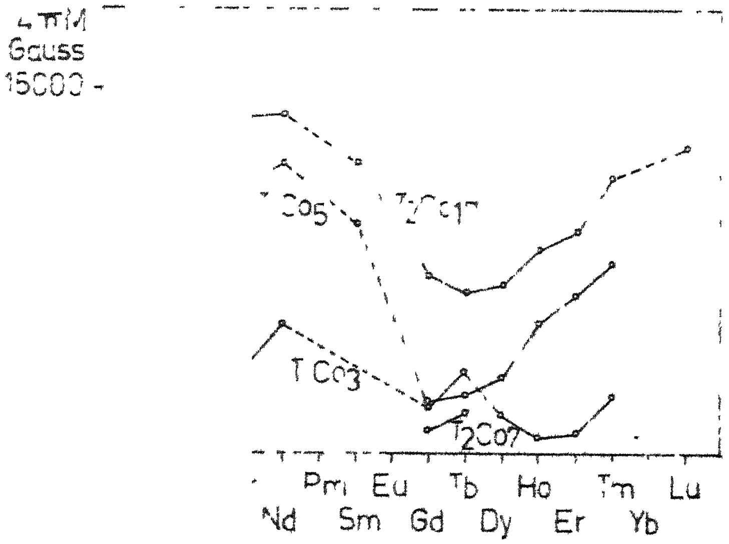

RATION INDUCTION OF SEVERAL
ARTH (T) COBALT (Co) PHASES (25)

TABLE I.4

Magnetic Properties of $RECo_5$ Compounds (1)

Compound	Saturation Magnetization $4\pi M_s$, KG	Anisotropy Field, H_A KOe	Theoretical Energy Product, $(BH)_{max}$, MGOe
YCo_5	10.6	130	28.1
Lanthanum	9.09	175	20.6
Cerium	7.7	170–210	14.8
Praseodymium	12.0	145–210	36.0
Samarium	9.65	210–290	23.0

Comparatively less amount of work has been done on the fabrication of magnets from the RE_2Co_{17} type compounds. Even though RE_2Co_{17} compounds have large saturation magnetizations and high Curie temperatures compared to the corresponding $RECo_5$ compounds (Figs. 1.6 and 1.7), efforts at producing magnets with good properties from the RE_2Co_{17} compounds were unsuccessful. This is because of the fact that RE_2Co_{17} compounds of light rare earths and Y, excepting Sm_2Co_{17}, exhibit easy magnetization directions lying on the basal plane and show weak or practically no anisotropy (26). Sm_2Co_{17} exhibits easy c-axis behaviour and also has high anisotropy (H_A = 105 KOe) (27). Consequently, much of the work done on the RE_2Co_{17} compounds has been with the Sm_2Co_{17} compound. Initial results indicate that the procedure employed in fabricating the $RECo_5$ type magnets may not be applicable for the fabrication of magnets from the RE_2Co_{17} compounds (8). This is probably because of the fact that the RE_2Co_{17} type compounds are not as brittle as the $RECo_5$ compounds and the process of powdering causes mechanical damage of the surface layers of the particles (28). At present, investigations are going on in several laboratories abroad to find the fabrication procedure for these RE_2Co_{17} compounds to achieve better magnetic properties.

Replacement of the light RE element by another in $RECo_5$ compounds has been studied for obtaining better magnetic properties. Through these studies it is revealed that one RE can replace another in the $RECo_5$ structure and a few light RE additions like Nd, Pr etc. improve the magnetic characteristics of the $RECo_5$ alloys. For example, an energy product of 23 MGOe has been reported for the (Sm, Pr) Co_5 alloy (7) whereas for the $SmCo_5$ alloy it is only 20 MGOe (6). No such studies are reported for the RE_2Co_{17} compounds.

Ternary alloys of AB_5 stoichiometry involving partial replacement of cobalt by one (non-ferromagnetic) or two (one non-ferromagnetic and other ferromagnetic) transition metals of the iron group have also been investigated for realizing better magnetic properties. Extraordinarily high coercive force values have been achieved for the RE $(Co_{1-x}Cu_x)_5$ alloys by a solid state precipitation of the magnetic $RECo_5$ phase in a non-magnetic $RECu_5$ matrix. For example, as cast $SmCo_5$ samples have coercivities less than 1000 Oe whereas the as cast $Sm(Co_{1-x}Cu_x)_5$ alloys with x=0.3 to 0.4 have coercivities as high as 10,500 Oe and it is further improved to 28,000 Oe after annealing at 400°C (29). Similar improvement in coercivity has been reported for the Al substituted $RECo_5$ alloys (29). While the coercivity increases due to the addition of non-magnetic elements in $RECo_5$ phase, the remanence is reported to decrease drastically (e.g. 9500 Gauss for $SmCo_5$ to 1000 Gauss for $SmCoCu_4$) because of the dilution of the matrix by the non-magnetic copper or allumnium (29). Small additions of iron to the Cu modified $SmCo_5$ compounds, however, are reported to increase the saturation magnetization as well as coercive force. For example, the annealed (425°C, 4 hrs) compound $Sm(Cu_{1.35}Fe_{0.5}Co_{3.5})$ showed a coercive force of 10,000 Oe which is 4000 Oe higher than that of the corresponding compound without iron addition. The saturation induction (5900 Gauss) of the Fe containing alloy is also higher (by about 500 Gauss) than the alloy with no Fe (29).

Several workers tried to replace cobalt by the relatively cheap and abundant 3d transition metal, iron. But no systematic investigation of the phase equilibria in the RE-Co-Fe system has been published. Only a few workers have investigated the limits of extension of the $RECo_5$ phase on addition of Fe (30). From their results it appears that the so called pseudo-binary compounds - $RECo_5$ with Fe, are unstable. This may be because of the fact that there is no compound corresponding to $RECo_5$ in the RE-Fe system (Fig. I.1). Buschow has investigated a limited composition range of the Sm-Co-Fe system (30). He observed an increase in saturation magnetization (92 emu/g for $SmCo_5$ to 117 emu/g for $SmFeCo_{4.7}$) and a decrease in intrinsic coercive force from 18 KOe to 10 KOe for a 1 hr. ball milled material. However, on continued ball milling of the material, the coercive force was reported to increase to about 14 KOe, a value very close to that of $SmCo_5$. Thus, the iron substituted $SmCo_5$ compounds have somewhat better magnetic properties than the compound without Fe.

No phase equilibria data is available for the substitution of Co by Fe in RE_2Co_{17} compounds. Ray et al (31) have mentioned that extensive solid solutions exist between RE_2Co_{17} and RE_2Fe_{17} phases at high temperatures. The $RE_2(Co_{1-x}Fe_x)_{17}$ phase, however, goes through an eutectoid transformation and at room temperature, stable $RE_2(Co_{1-x}Fe_x)_{17}$ phases are restricted only to the neighbourhood of the binary compounds. They observed that the $RE_2(Co_{1-x}Fe_x)_{17}$, however, can be retained in a metastable state by quenching (3). Magnetic measurements were carried out with the metastable samples of the $Sm_2(Co_{1-x}Fe_x)_{17}$ alloys in which x varies from 0 to 1 (32). The values of T_c, $4\pi M_s$ and H_A for these alloys are plotted as a function of x in Fig. I.8. As shown in the figure, the Curie temperatures of these alloys remain above the T_c of $SmCo_5$ when Fe is substituted for Co upto about x=0.6. The saturation magnetization increases on the addition of Fe and goes through a maximum on the iron-rich side before it declines. A similar behaviour is reported for $Y_2(Co_{1-x}Fe_x)_{17}$ alloys (8). This is quite analogous to the behaviour of binary Fe-Co alloys. The desirable easy c-axis behaviour is maintained upto about 50 percent iron

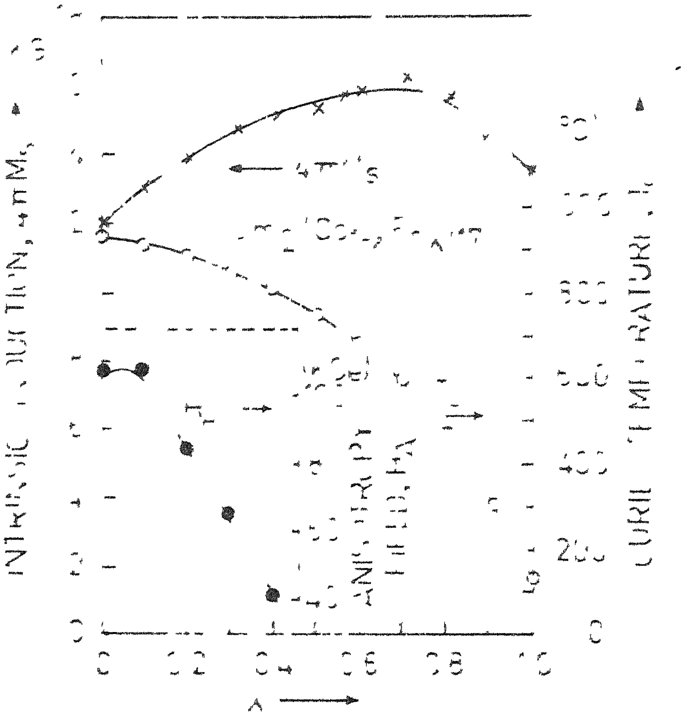

FIG I 8 VALUES OF $4\pi M_s$, T_c, AND H_A FOR THE $Sm_2(Co, Fe)_{17}$ ALLOYS (32)

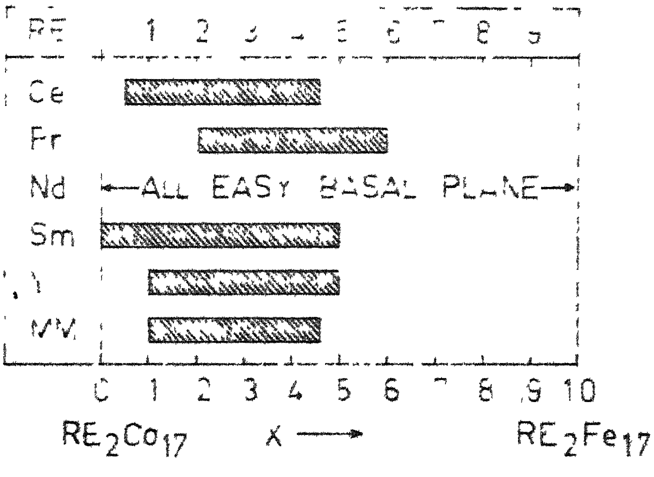

I 9 MAGNETIC SYMMETRY OF THE $RE_2(Co_{1-x}Fe_x)_{17}$ PHASES (32) substitution in the $Sm_2(Co_{1-x}Fe_x)_{17}$ alloys, as shown in Fig. I.9. Also, the substitution of iron first enhances the easy axis anisotropy (H_A) of Sm_2Co_{17}, H_A then drops, but remains attractively high upto about x=0.4. In the case of pseudo-binary RE_2Co_{17} – RE_2Fe_{17} systems of other rare earths Ce, Pr and Y, the most remarkable feature of Fe addition is that between 5 to 20 percent Fe substitution for Co, the c-axis becomes the easy axis of magnetization and this is maintained upto about 45 to 60 percent Fe substitution (Fig. I.9). The maximum values of the anisotropy field in these cases are, however, substantially lower than those of $Sm_2(Co_{1-x}Fe_x)_{17}$ alloys (less than 20 KOe) (32). Thus, the $Sm_2(Co_{1-x}Fe_x)_{17}$ alloys with x=0 to 0.4 are clearly superior to the others. Early attempts to produce A_2B_{17} type magnets have therefore correctly concentrated on the $Sm_2(Co_{1-x}Fe_x)_{17}$ phase between $0 < x < 0.4$. It is predicted that magnets with $(BH)_{max}$ values as high as about 60 MGOe will be possible to obtain with the $Sm_2(Co_{1-x}Fe_x)_{17}$ alloys.

Extensive data is available on the solubility of rare earths among themselves. Complete solid solubility in the Ce-La, La-Nd and Pr-Nd systems and extended solubility for the other rare earths among themselves has been reported(33). Thus, it is expected that in all the RE elements will be in solid solution form and when alloyed with other elements the

MM will behave like a single RE element. This behaviour has been observed in the MM-Mg system which exactly resembles the (Ce, La, Nd) - Mg systems (34). No such data is, however, available for the MM-Co and MM-Fe systems but, it may safely be assumed that MM-transitional metal systems will show a behaviour similar to the MM-Mg system.

Even though no phase equilibria data is available for the MM-Co system, several workers have investigated the magnetic properties of $MMCo_5$ phase (MM in these cases had rare earth contents of 45-60 at percent Ce, 23-35 at percent La, 9-20 at percent Nd and 3-7 at percent Pr). Strnat et al (35) and McCaig (36) obtained a $(BH)_{max}$ value of 2.3 MGOe for the field pressed $MMCo_5$ powder without sintering. Later, by using sintering techniques, Johnson and Fellows (37) and Das (38) achieved a $(BH)_{max}$ value of 9 MGOe for the $MMCo_5$ magnets. No magnetic data is available for the corresponding MM_2Co_{17} compounds excepting that the MM_2Co_{17} compound is reported to have the easy axis of magnetization in the basal plane (26).

Small additions of other rare earths are reported to vastly improve the magnetic properties of $(MM_{1-x}RE_x)Co_5$ compounds. Several workers have investigated the system $(MM_{1-x}Sm_x)Co_5$ for x = 0 to 1 and found that the magnetic properties steadily improved with Sm additions (38,39,40). For example, $(BH)_{max}$ value for $MMCo_5$ is reported to be

14.5 MGOe whereas for $MM_{0.5}$ $Sm_{0.5}$ Co_5, it is reported to be 18 MGOe (39). The effects of other rare earth additions like Ce, Pr, Nd, La have also been studied. For this purpose, Nagel and Meuth (39) selected a composition $(MM_{1-x}RE_x)_{0.85}$ $Sm_{0.15}$ Co_5 with $0 < x < 0.5$. Their results can be summarized in the following way: (1) Ce reduces the ${}_{M}H_c$, H_A and B_R. M_s is also slightly lowered; (2) La increases the ${}_{M}H_c$, slightly decreases the H_A but does not change the B_R and M_s; (3) Pr reduces the ${}_{M}H_c$ and H_A but increases the B_R and M_s; (4) in the case of Nd, ${}_{M}H_c$ is reported to **increase initially** (from 8 KOe at 0 percent Nd to 16 KOe at 10 percent Nd) but further additions of Nd decrease the ${}_{M}H_c$. H_A is reported to decrease steadily with increase in Nd content. Both B_R and M_s are reported to increase with Nd additions. From these results, Nagel and Meuth report that energy products upto 18 MGOe can be obtained with MM based magnets.

Cast permanent magnets based on MM $(Co, Cu)_5$ alloys, in which magnetic hardening is produced by solid state precipitation of a magnetic phase in a non-magnetic matrix, have also been produced and studied for their magnetic properties. Strnat et al (41) and Takata (42) obtained an energy product of 6 MGOe for the cast MM $(Co,Cu)_5$ magnets. Later, by using powder metallurgy techniques, higher energy product (~ 8 MGOe) magnets have been developed from

MM$(Co,Cu)_5$ alloys (43). Iron additions to MM$(Co,Cu)_5$ alloys are found to further improve the magnetic properties (44).

No magnetic data is available for both MM$(Co,Fe)_5$ and MM$_2(Co,Fe)_{17}$ alloys. However, iron additions of about 10 percent are found to change the easy axis of magnetization from the basal plane to the c-axis (Fig. I.9) in the MM$_2(Co_{1-x}Fe_x)_{17}$ alloys and this c-axis magnetic symmetry is maintained upto about x=0.45.

I.2 Statement of Problem:

The use of iron and mischmetal substantially reduces the cast of RE-Co magnets even though their use may lead to somewhat inferior magnetic properties compared to those of the $SmCo_5$ magnets. However, as mentioned in section I. , for certain applications, magnetic properties comparable to those of $SmCo_5$ magnets are not really necessary. Consequently, in such applications, the MM-Co and the MM-(Co, Fe) alloys have definite economic advantage over other materials.

The ferromagnetism in transition metals Fe, Co and Ni is due to unequal filling up of the 3d sub-bands. Addition of Fe to Co (Fe having one less electron/atom than Co) causes more imbalance between the two 3d half bands of Co and as a result magnetic moment/atom increases as Fe content is increased. The moment/atom goes through a maximum near about 70 percent Fe. A similar effect has been observed with the RE-Co systems - addition of RE appears to reduce the imbalance in the two half bands thereby lowering magnetic moment/atom of the transition metal (25). On Fe addition to $RECo_5$ and RE_2Co_{17} phases of Gd-(Co,Fe), Y-(Co,Fe) and Sm-(Co,Fe) systems, it has been reported (8,32,45) that magnetization increases with increase in Fe and it passes through a maximum at a reasonably high Fe content, similar to what has been found in the Fe-Co system. On the basis of these observations, it is expected that in MM-Co-Fe system also, there will be an increase in magnetization with increase in Fe. Moreover, there may be new phases existing in the RE-Co-Fe system with magnetic properties similar or superior to the $MMCo_5$ and MM_2Co_{17} phases. With these points in view, it was thought necessary to carry out the phase equilibria work in the MM-Co-Fe system. As mentioned in the last section, only compounds of the type AB_5 and A_2B_{17} are of importance for permanent magnet applications. However, it was reported (46,47,48) that optimum properties of sintered $RECo_5$ magnets were attained only if the starting material was hyper stoichiometric, i.e., contain a few percent of the RE_2Co_7 phase. So, the study of MM-Co-Fe system was restricted to the composition range between $MM_2(Co,Fe)_7$ to $MM_2(Co,Fe)_{17}$.

The phase equilibria work is expected to show the different phases that coexist in the MM-Co-Fe system. Of these only a few may be of importance for permanent magnets. Curie temperature is an important magnetic characteristic of permanent magnetic materials. Hence, to get a first hand information on which alloys have favourable magnetic characteristics, it was decided to determine the Curie temperatures of various RE-Co-Fe alloys. Since it is known that the Fe addition affects the magnetic easy axis of the A_2B_{17} type phase, it was also felt that the easy magnetization axis of the known and the new phases in the MM-Co-Fe system should be determined as a function of Fe content.

In the fabrication of RE-Co magnets, various techniques like sintering, liquid phase sintering etc. are used for developing optimum properties. To choose suitable sintering and annealing temperatures for the ternary MM-Co-Fe alloys, a knowledge of the melting points of various alloy compositions is very essential. Thermal analysis methods are suitable for this purpose. Hence, a high temperature thermal analysis apparatus was considered to be set up for determining the melting points of the MM-Co-Fe alloys.

CHAPTER II

THERMAL ANALYSIS APPARATUS

Since in the fabrication of the magnets the ternary alloys of mischmetal, cobalt and iron are to be used, a knowledge of their melting points is necessary for choosing suitable sintering temperatures. Thermal analysis methods are suitable for establishing the solid-liquid transition temperatures. Hence, a thermal analysis facility was set up.

II.1 Design and Description of Apparatus:

For ease of detecting the thermal arrest produced during thermal analysis, a large amount of sample and slow heating and cooling rates have to be used. In the present investigation of the RE-Co-Fe systems it was expected that only small amounts of materials would be available for thermal analysis. Hence, a thermal analysis apparatus which would be sensitive enough to show reasonably large thermal arrests even with small amounts of materials was required to be built. An already fabricated water-cooled furnace chamber(49) suitable for use with high vacuum as well as with inert gas atmosphere, was available for conversion into a thermal analysis apparatus. As shown in Fig. II.1, the chamber was in three parts - a bottom plate, a central cylindrical section and a top plate. A small furnace, 1 1/4" dia x 1½" long, was

FIG.II.1 THERMAL ANALYSIS APPARATUS

1. Cylindrical Portion of the Brass Chamber
2. Cooling Coil
3. O-ring Joint through which the T-tube is connected
4. Top Plate of the Brass Chamber
5. Brass Flange
6. O-ring Joint through which the Thermocouple is inserted.
7. Stainless Steel Thermocouple Protection Sheath
8. Holder for the Gas Head
9. Gas Head Outlet
10. Stainless Steel Tube-Gas Head
11. Gas Head-Inlet
12. Thermocouple Leads
13. Connectors
14. Holder for Thermocouple Cold Junction Leads
15. Thermocouple Cold Junction Leads.
16. Cooling Coil
17. Stainless Steel Radiation Shields with Top Covering Plates

18 and

19. Recrystallised Alumina Furnace Cores
20. Sintered Alumina Crucible
21. Heater Element - Mo
22. Short-circuited Furnace Leads.
23. Alumina Tube Supporting the Platform
24. Alumina Thermocouple Protection Sheath
25. Alumina Cement on Furnace Windings
26. Furnace Leads
27. Mo-Radiation Shield with Cover
28. Sintered Alumina Platform
29. Fire Clay Support
30. Stainless Steel Radiation Shields
31. Stainless Steel Connector
32. Brass grooves for holding the Alumina Tubes
33. Glass to Metal Seals
34. Furnace Leads
35. Levelling Screw Base
36. Levelling Screws
37. Gas Inlet for the Brass Chamber
38. Brass Flange
39. Bottom Plate of the Brass Chamber
40. Fire Clay Support
41. Graphite Rods
42. Material

mounted on a sintered alumina platform supported by 3 rec 5 1/3 O.D. x 2½" long alumina tubes fixed to the bottom plate. Power to the furnace was fed through glass to metal seals fixed to the bottom plate. Five concentric radiation shields with top covers having ½" dia central holes and two bottom radiation shields, all made of stainless steel, completely surrounded the furnace to minimize heat loss. A thin Mo radiation shield with a cover having a 3/16" dia central hole was used next to the furnace to protect the stainless steel radiation shields. For the purpose of thermal analysis of the sample, a Pt-Pt + 10 percent Rh thermocouple was inserted through the top plate.

The furnace had to be designed on the basis of the requirement that if should work at temperatures in the range of 1000°C to 1400°C (or 1600°C) in inert atmosphere or high vacuum and that it should be possible to get heating and cooling rates as small as desired. The choice of material for the furnace was limited to only a few materials like Ta, Mo and Pt-Rh alloys. Of these, only Ta and Mo were tried. Since a small furnace with sufficient electrical resistance was desired, Ta (which has higher specific resistance than Mo) was first chosen even though its use necessitated the use of high vacuum. Soft, annealed 0.02" dia Ta wire was rolled into a strip of 0.008' thickness and a furnace with 2.5 Ω total resistance was fabricated. The difficulties with this furnace were that (1) it needed maintenance of high vacuum ($4x10^{-5}$ mm Hg or better) for a long time, (2) since the furnace had to be heated slowly, time of operation lengthened and (3) long period in high vacuum caused large volatilization of material. Since the Ta furnace failed to operate satisfactorily, Mo winding was tried. The available Mo wire was of 0.025" dia. and was comparatively more stiff than the available Ta wire. Because of this the Mo wire could not be rolled down to a thin strip of higher resistance. A Mo wound furnace of the same size as the Ta furnace gave a total resistance of only 1 Ω and the control of heating or cooling rate was found difficult. To increase the electrical resistance of the furnace, two concentric Mo wound furnaces connected in series were tried. Two recrystallized alumina tubes (cylindrical parts of recrystallized alumina crucibles) of 1" O.D. x 1½" long and 1 1/4" O.D. x 1 1/8" long respectively were used for making the two furnaces. They were put concentrically and connected in series using a stainless steel connector. The total resistance of this two-layer furnace was about 3 Ω.

In the initial runs at high temperatures (1300°C to 1400°C), the Pt vs Pt + 10 percent Rh thermal analysis thermocouple got stuck to the locally made alumina protection sheath kept in the melt and the thermocouple wires snapped during its removal from the sheath. To avoid this, it was necessary to keep the thermocouple in a tube which could be kept in the alumina sheath so that no damage is done to the thermocouple. Thin walled pure alumina tube of 1/8" would have been the ideal choice. But, since it was not available, a thin walled (0.01" wall thickness) stainless steel tube of 1/8" dia, closed at one end by fusing it, was used. The use of stainless steel tube, however, restricted the operation of the furnace upto 1400°C. The thermocouple was insulated from the stainless steel tube by putting thin Al_2O_3 sleeves on the wires and by keeping the hot junction in alumina powder put at the bottom of the stainless steel tube. The thin stainless steel tube, if exposed to atmosphere at high temperatures, was expected to oxidise and fail. So, it was connected to a gas head made of brass for flowing argon gas. Purified argon gas was inserted into the stainless steel tube through a syringe needle. The stainless steel tube-gas head was supported by a holder as shown in Fig. II.1.

The Mo furnace requires an inert atmosphere for its operation. Argon gas purified by passing of over hot copper turnings and titanium chips was used for this purpose. The gas was inserted through the bottom plate into the chamber and let out from the side of the furnace chamber through an oil bubbler. For ensuring that all the air was replaced by argon gas before heating the furnace, a vacuum pump was connected to the system as shown in Fig. II.2. The furnace chamber

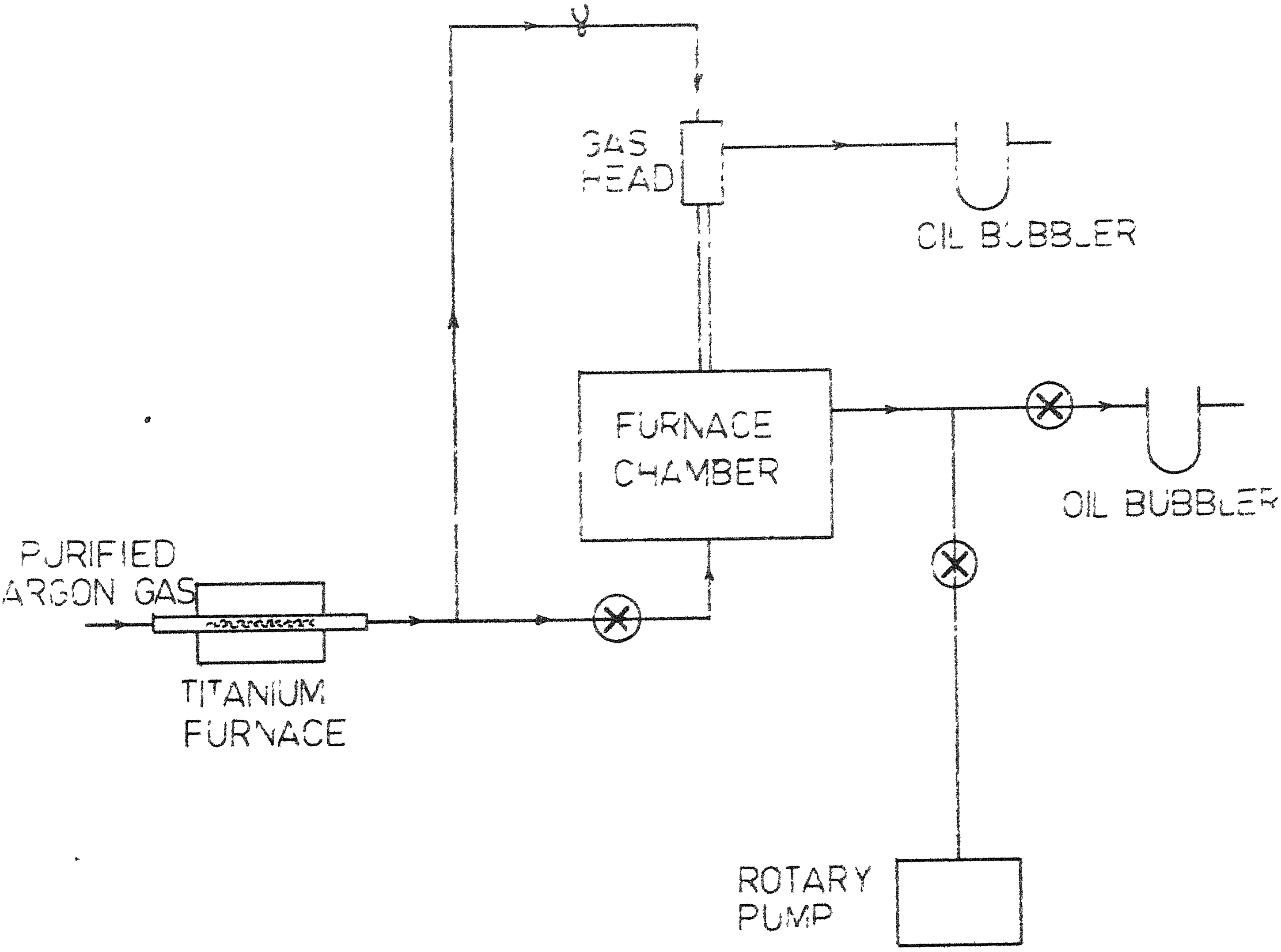

DIAGRAM REPRESENTING THERMAL SIS SET-UP

was evacuated to about 20µ Hg and argon was flushed through the system 2 or 3 times before commencing heating of the furnace.

Since small amount of material was to be used for thermal analysis, the total amount of heat liberated or absorbed at the transformation point was expected to be small. The small heat effect was expected to make the thermal arrest of short duration and with relatively large heating or cooling rate (eg. 2°C/min) it might not be possible to see clearly the small thermal arrest. Because of this, very small heating or cooling rate ($\simeq$0.5°C/min) was desired. The total resistance of the furnace being small, a very fine control of voltage was necessary to obtain slow heating and cooling rates This was achieved through an arrangement shown in Fig. II.3. A stabilized stepped down voltage was fed to three Dimmerstats set in tandem, the first two were used to step down the input voltage suitably so as to get fine voltage control over the whole range of the Dimmerstat and the third one was used to increase or decrease the set voltage by small amounts.

For thermal analysis, the output of the thermocouple was fed to a recorder through a cold junction (melting point of ice) so that the changing mv, corresponding to the changing temperature, with time could be recorded directly. The mv generated by the thermocouple in the useful temperature range was between 8 to 14 mv. So, one could directly use a

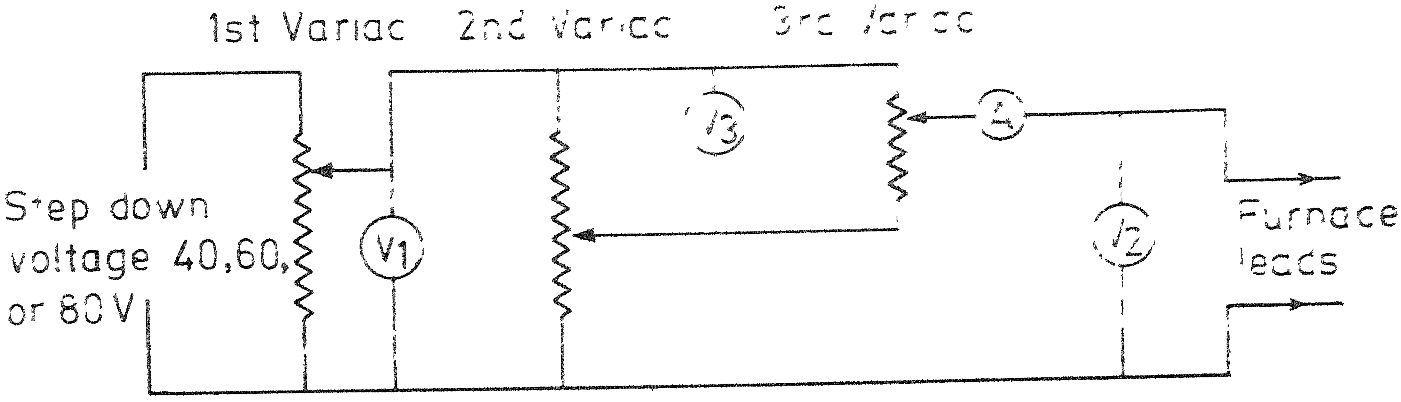

FIG II 3 FURNACE POWER SUPPLY CIRCUIT

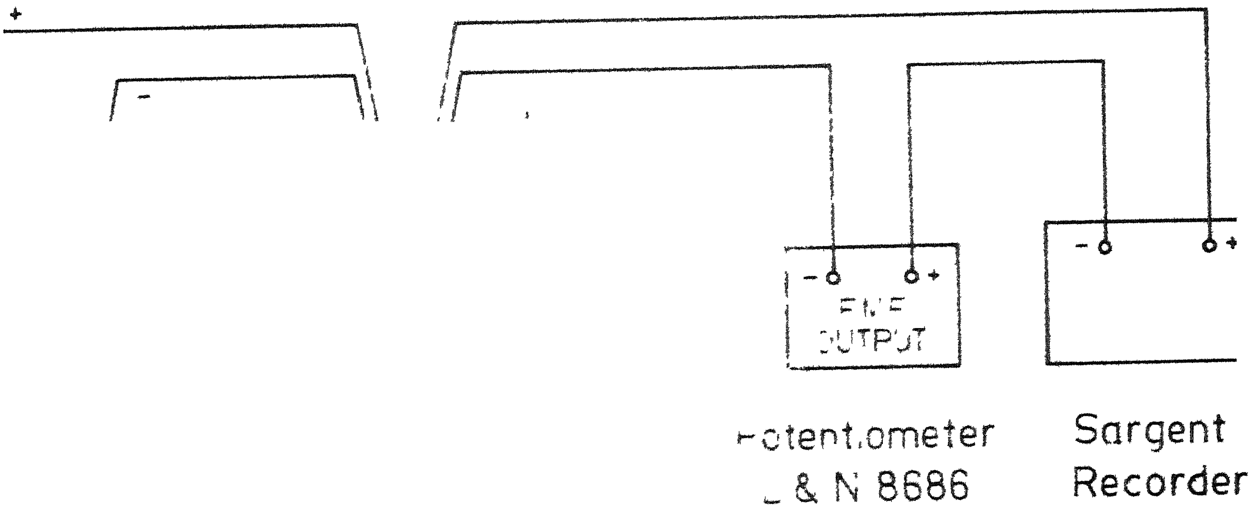

UTPUT MEASUREMENT CIRCUIT

recorder with full scale deflection of 10 or 20 mv and record the thermal arrest. However, the large recorder range required (0-10 or 0-20 mv full scale) made the measurement rather inaccurate because the change in mv per unit time was rather low (≃ 0.01 mv/min) at the transformation point. Hence, it was thought to make the measuring circuit more sensitive. Since the major part of the mv reading was useless for our purpose, it was thought that if an emf of known value was fed against the thermocouple emf and was kept constant throughout the experiment, then a more sensitive scale such as 0-1 mv range could be used. A Leeds and Northrup, Model 8686 potentiometer was used through which a predetermined emf could be fed against the thermocouple emf. The accuracy of the potentiometer is ± 0.007 mv and hence, a very fine control of emf was possible. The unbalanced emf of this system was fed to a Sargent recorder (Fig. II.4) with a 10" chart span and with 0-1 mv full scale deflection.

The RE-Co alloys are reported to react with Al_2O_3 crucibles (50). Commercially available Al_2O_3 crucibles, which are usually sintered at low temperatures (≤ 1400°C), are very porous and cannot be used. But, since no other suitable crucible material was available, it was considered to use Al_2O_3 crucibles sintered at higher temperatures. The facilities available in the Institute were used for this purpose. 99.9 percent pure Al_2O_3 powder (≃ 5μm in size) was blended with water and for optimum plasticity of the material, the blend was maintained at a pH of 3-4 using HCl. The crucibles and sheaths of required sizes were made by slip casting the blended alumina in plaster of paris moulds. An allowance of about 30 percent was given for shrinkage during sintering. The cast crucibles and sheaths were presintered at 1000°C for 10 hrs. After machining, if necessary, the presintered crucibles final sintering was done at 1700°C for 2 hrs in a zirconia pot furnace. Crucibles of high density and wall thickness of 1/16" could be prepared by this sintering operation.

II.2 Testing and Calibration:

Initially blank runs were made to find the voltage - temperature characteristics of the thermal analysis set up and to determine how slow heating and cooling rates could be achieved with the two-layer furnace assembly. The power supply to the furnace was raised in steps of 2 volts and the furnace was allowed to stabilise its temperature before each successive increase of input voltage. The temperatures attained corresponding to different voltages are listed in a Table in Appendix I. In the low temperature region (upto about 800°C), the furnace usually took about 8-12 minutes to stabilize its temperature after every increment in voltage (2 volts) whereas in the high temperature region ($>$ 800°C) the time to stabilize temperature was about 4-8 hrs. On the whole, the temperature of the furnace was raised at the rate of 3-4°C/min. After attaining the desired temperature the desired cooling or heating rates were obtained by slightly raising or lowering the applied voltage to the furnace. The heating and cooling rates could be controlled effectively by this method. For example, a change of the voltage by about 0.6 volts at 1000°C produced a heating rate of about 1°C/min. Similarly, for obtaining a cooling rate of 1°C/min around the same temperature, a voltage change of about 0.5 volts was needed. For slower heating or cooling rates, smaller voltage changes 0.2-0.4 volts were needed. A change of voltage by about 0.3 volts produced a heating rate of 0.5°C/min and the same cooling rate needed a change of input voltage by about 0.25 volts. The slowest heating or cooling rate achieved was about 0.4°C/min. Still slower heating or cooling rates could not be achieved for the following reasons: (1) when voltage lower than 5V was impressed or the third Dimmerstat, the heating or cooling rates could not be controlled, (2) since voltmeters of smaller range (0-1 V) were not available, the voltage changes could not be measured accurately. At higher temperatures (1300°C and more) control of heating and cooling rates was relatively easy because of the increase in furnace resistance.

After initial testing of the furnace assembly, a test run with one of the calibrating specimens (Germanium) was made. 15 gm of 99.9 percent pure germanium, obtained from Semi Elements Inc., N.Y., U.S.A., was kept in a $\frac{1}{2}$" I.D.x1" long Al_2O_3 crucible supplied by Headway Ceramics, Varanasi. A small fused silica sheath was used, for protecting the thermocouple from coming in contact with the material. It was inserted into the material and then the crucible was kept in the furnace. The furnace chamber was assembled and the thermocouple was inserted through the top plate. The system was evacuated to about 20μ Hg pressure and flushed with purified argon gas 3,4 times. The chamber was finally filled with purified argon gas. During the run, purified argon gas was allowed to flow through the chamber as well as the thermocouple assembly and bubbled through the oil bubblers at a rate of 4 to 5 bubbles/min and 1 bubble/min respectively. Since about 45 volts supply was needed to raise the furnace temperature to about 960°C (see Appendix I), a stabilised stepped down voltage of 60V was fed to the first Dimmerstat and the second Dimmerstat (with 45V input voltage) was then continuously monitored to raise the temperature of furnace at a rate of 4-5°C/min. The third Dimmerstat was set at zero during the initial heating up of the furnace. It was ensured that the furnace chamber was properly cooled during heating up of the furnace. Ice was put in the thermocouple cold junction bath. The strip chart recorder was calibrated and connected to the thermocouple emf measuring circuit. The furnace temperature was raised to about 910°C using the second Dimmerstat. Then the differential voltage (~ 5V) from the third Dimmerstat was used for further slow heating and cooling. In the first run, a heating rate of 2°C/min was used and the output emf was plotted on the recorder. A small thermal arrest was seen around 8.85 mv emf output (corresponding to about 940°C). So, the furnace was allowed to rise to only 950°C. Then it was cooled slowly at a rate of 1.5°C/min. This time, a comparatively large thermal arrest was found at 8.86 mv. To make the thermal arrest still larger, slower heating and cooling rates (1°C/min, 0.5°C/min and 0.4°C/min) were used and the time temperature curves were traced on the recorder. A small variation in the emf of the arrest point, ± 0.015 mv around the mean value, 8.85 mv, was found in different heating and cooling cycles. A cooling curve obtained with 0.4°C/min cooling rate is shown in Fig. II.5(a). After the thermal analysis runs were made, before shutting off the furnace power, the valves near the oil-bubblers were closed. This was done to prevent sucking up of oil into the furnace chamber or into the thermocouple assembly during cooling of the furnace. Then, the furnace was allowed to cool by putting

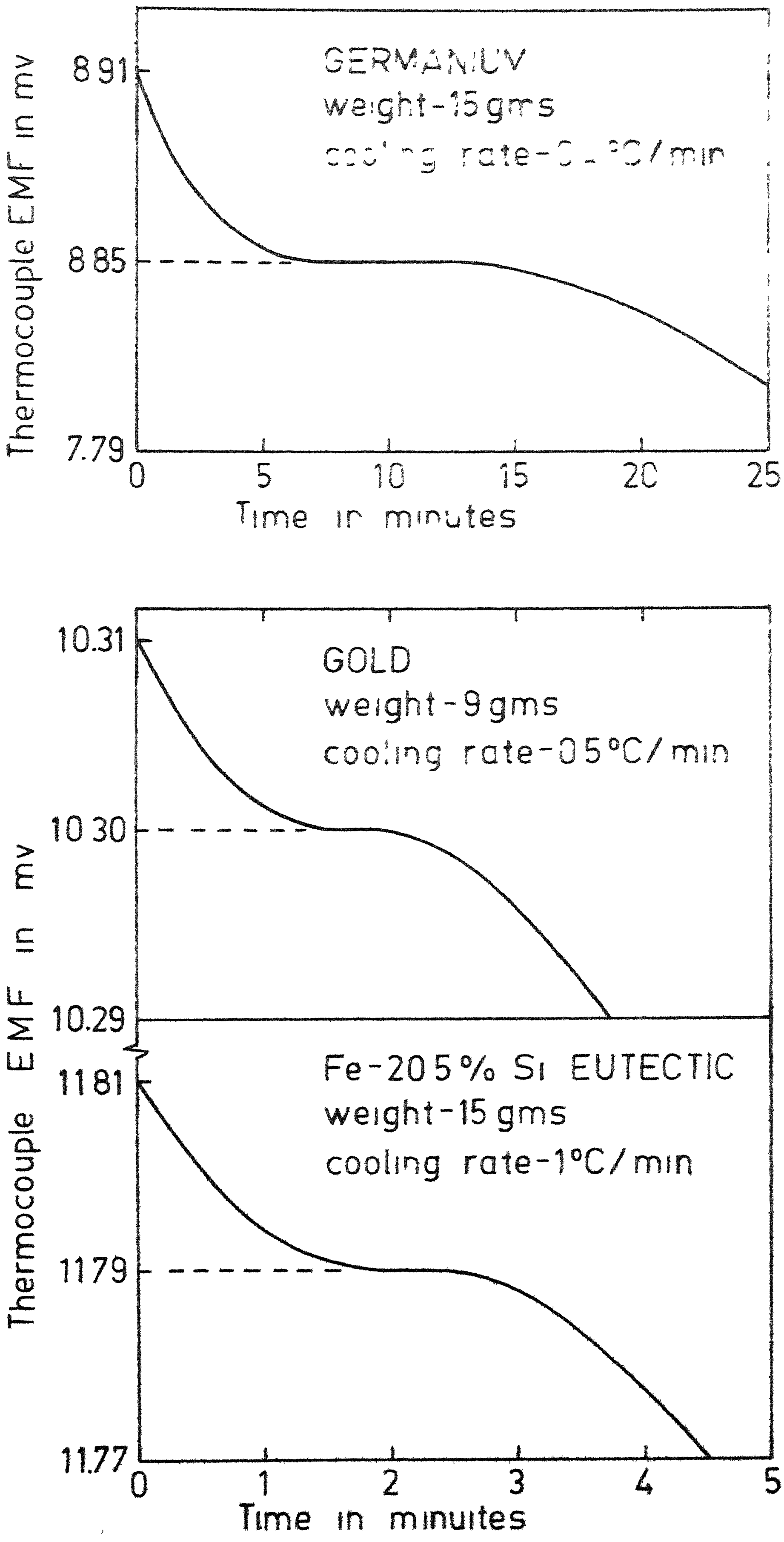

FIG. II 5 TYPICAL COOLING CURVES:
(a) Germanium (b) Gold (c) Fe-Si eutectic

off the power supply.

Calibration is usually made against the melting points of pure metals. For calibrating the thermocouple in the temperature range of interest (1000°C-1400°C), germanium and gold having melting points 937.4°C and 1063°C were used. The third calibration was planned with silicon having a melting point of 1410°C. But, due to the use of stainless steel thermocouple sheath, silicon could not be used as a calibration material because the melting point of stainless steel ($\simeq$ 1420°C) is very close to the melting point of silicon. Since no other non-reactive pure metal with accurately known melting point in the temperature range of 1100°C and 1400°C was available, it became necessary to use an eutectic alloy of known **eutectic** point. Fe-20.5 wt. percent Si eutectic was found suitable for the present work. There is some uncertainty in the reported eutectic temperatures of Fe-Si (20 wt percent) alloy. Haughton and Becker (51), using high purity materials, reported an eutectic temperature of 1195°C for Fe-20 wt. percent Si. Murakami reported a temperature of 1205°C for Fe-23 wt percent Si (52). Phragmen (53) and Osawa et al. (54) reported an eutectic temperature of 1200°C for the Fe-21.2 wt percent Si and Fe-22 wt percent Si alloys respectively. On the basis of these data Hanson and Anderko (55) has shown the eutectic temperature as 1200°C.

The same temperature with a possible uncertainty of ±5°C has been used in this calibration as the eutectic temperature of Fe-20.5 wt percent Si. About 15 gm of the eutectic alloy was prepared by arc melting electrolytic iron flakes obtained from Gallard Schelsinger Mfg., Co., N.Y., U.S.A. and silicon obtained from Semi Elements Inc., N.Y. U.S.A.

In the case of Ge and the Fe-Si alloy, the arrest points were found to drift somewhat and hence mean values of thermal arrest emf of all the heating and cooling runs were used for thermocouple calibration. For gold, no variation in the arrest point was observed (Table II.1). With the help of the known melting temperatures and the thermocouple emf values corresponding to the thermal arrests, a calibration curve, Fig. II.6, was drawn. Since there was some drift observed in the thermal arrests of Ge and Fe-Si alloy and because there was a small uncertainty in the melting point of Fe-Si alloy (uncertainty limits are shown by horizontal and vertical bars in Fig. II.6) the temperature measured with the help of the thermocouple will have a small uncertainty. It is, however, clear from the calibration curve that this uncertainty is small, about ±5°C. The thermocouple was calibrated only in the temperature range 930°C to 1200°C. However, from the smoothness of the calibration curve, it is expected that it can be extended safely to about 1350°C or 1400°C.

TABLE II.1

Thermocouple Calibration Data

Serial No.	Material	Thermocouple EMF corresponding to the melting point of the material	Melting Point
1	Germanium	8.85±0.015 mv	937.4°C
2	Gold	10.3 mv	1063°C
3	Fe-20.5 wt per-cent Si eutectic	11.785±0.025 mv	1200°±5°C

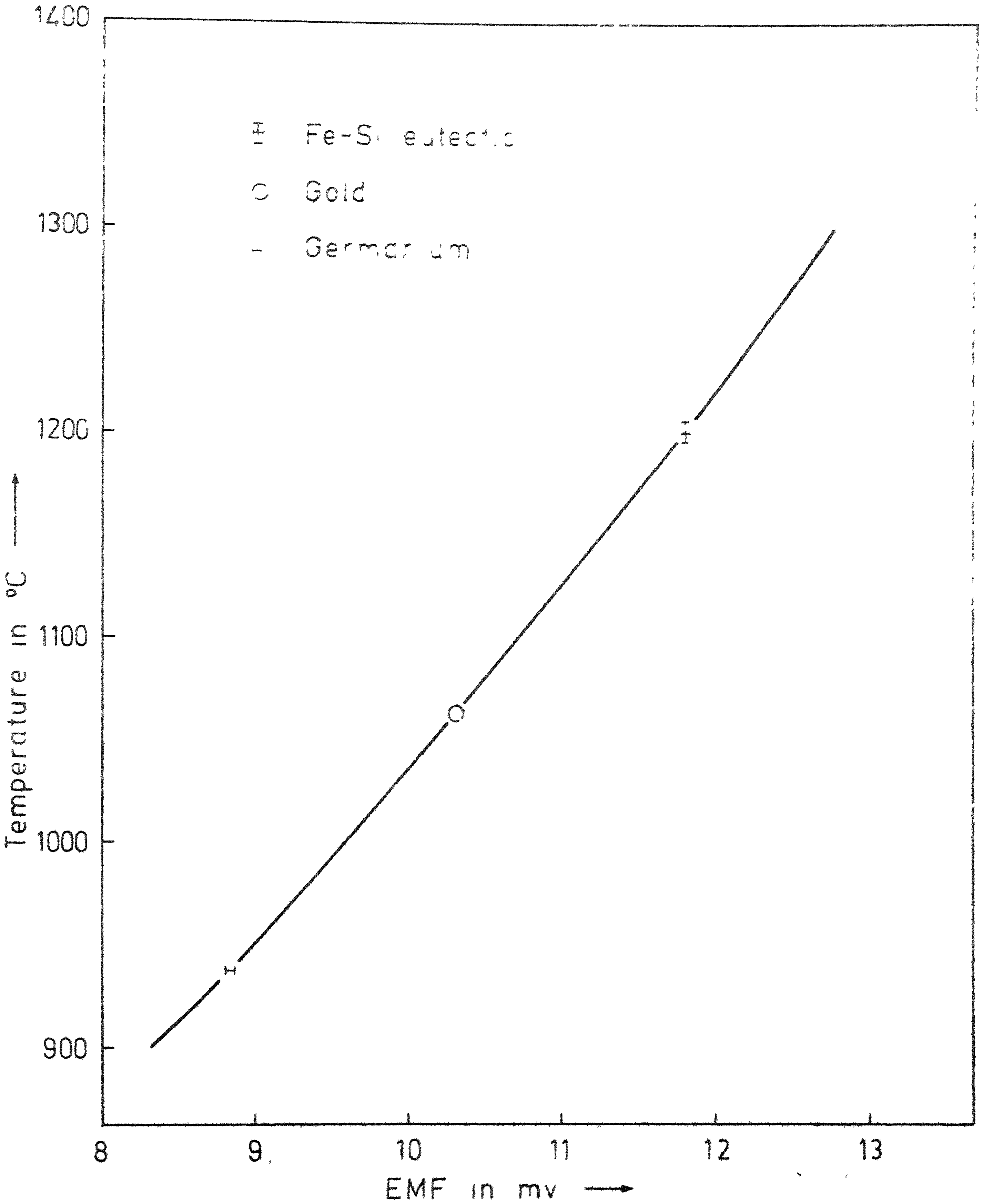

FIG. II.6. THERMOCOUPLE CALIBRATION CURVE

CHAPTER III

EXPERIMENTAL PROCEDURE

The present investigation involved the determination of

1. Phase equilibria in RE-Co-Fe system
2. Solidus and liquidus temperatures of the alloys (Thermal Analysis)
3. Curie Temperatures

and 4. Easy axis of magnetization

III.1 Phase Equilibria in RE-Co-Fe System:

For establishing the phase equilibria in RE-Co-Fe system, the experimental procedure followed consisted of the following steps: a) Melting of alloy, b) Annealing, c) Metallographic analysis, and d) X-ray diffraction analysis.

Melting:

Materials Preparation: The alloys were prepared by using 1) Mischmetal supplied by Mischmetal and Flints Pvt. Ltd., Alleppey, Kerala, India, containing 85-90 wt percent Rare Earth (RE), 6-10 wt percent Iron (Fe) and 1-4 wt percent impurities and the rare earth composition was Ce: 45-50 wt percent; La: 20-25 wt percent; Nd: 15-20 wt percent; Pr: 4-6 wt percent; Sm: 1-4 wt percent; Y and others: 1-2 wt percent,

ii) Cobalt (99.9 percent) supplied by Semi Elements Inc., N.Y., U.S.A. and iii) Electrolytic iron flakes (99.9 percent) supplied by Gallard Schelsinger Mfg. Co., N.Y., U.S.A. Since the exact amounts of individual rare earth elements in mischmetal were not known, an average composition was assumed basing on the supplier's analysis given above. The average composition used for calculating the rare earth molecular weight in mischmetal (MM) was 90 wt percent total RE; 8 wt percent Fe and 2 wt percent impurities and the individual rare earth compositions were 49.21 wt percent Ce, 23.31 wt percent La, 18.13 wt percent Nd, 5.13 wt percent Pr, 2.59 wt percent Sm and 1.55 wt percent Y. The calculated rare earth molecular weight on this basis was 140.11 gms. This molecular weight of RE was used in all calculations of the amounts of RE to be taken for different alloy compositions.

The mischmetal as supplied was in the form of biscuits coated with grease to protect it from atmospheric oxidation. Before cutting the mischmetal to pieces of required size, the grease was removed using acetone. The cut pieces were then ground to remove any oxide layer that was present. The pieces were weighed according to the alloy composition so as to make the total amount of alloy between 25 and 30 gms and the weighed pieces were kept in acetone till they were used for melting. Cobalt was in the form of a cast button and it was crushed to pieces of required size using a hammer. Iron was in the form of flakes; they were ground to remove the traces of rust. The amounts of iron and cobalt required for a given melt were weighed out and kept separately till required for melting.

Melting Furnace: The factors to be considered in a melting operation are : melting points of the elements, amount of material to be melted, reactivity of the components, contamination from crucible material. The melting points of the three components in RE-Co-Fe alloys are Mm: 900°C, Fe:1539°C and Co:1492°C. Out of these three metals, misch-metal is very reactive and is reported to react with even alumina crucibles (50). So, it was thought proper to carry-out the melting under protective argon atmosphere and without using a refractory crucible. A water cooled copper hearth arc furnace with non-consumable tungsten electrode was considered to be the best melting furnace. An available D.C. arc furnace was thus made use of for melting the RE-Co-Fe alloys. The crucible and the electrode were enclosed in a glass chamber which could be evacuated and an inert gas atmosphere could be maintained in it. The electrode was fitted to the top metal part of the glass chamber through O-ring joints so that the electrode could be raised or lowered with the help of a screw. This was necessary to adjust the gap between the electrode and the charge (usually kept between 1/8" to 1/4") so that arc could be struck without touching the charge with the electrode. It ensured clean, contamination free melting. A D.C. arc welder (1000 amp., 40 V) was used as the arc power supply. The different controls - start and weld controls - varying the welding current from 300 amps at 0 to 1000 amps at 100 on the control dial were available. With the help of these controls the arc pressure could be controlled. An automatic timer (0-180 secs) which could be set according to the required duration of melting was also available in the welder start circuit so as to shut off the arc current after a pre-selected time.

Gas Purification System: The common bottled argon gas contains moisture and oxygen both of which are detrimental to the Rare Earth alloys. Hence, it had to be further purified before putting it into the arc furnace chamber. For this purpose, a gas purification system was constructured. As shown in the block diagram (Fig. III.1), it consisted of several $CaCl_2$ and P_2O_5 absorber tubes and furnaces with Cu turnings and Ti chips. The Cu turnings and the Ti chips were kept in four ½" dia x 30" long quartz tubes over a length of 6" . The quartz tubes, in turn, were kept in a 2" dia x 15" long nichrome-wound furnace. The furnace was kept at 700°C so that the titanium remained in the α state (because it has higher

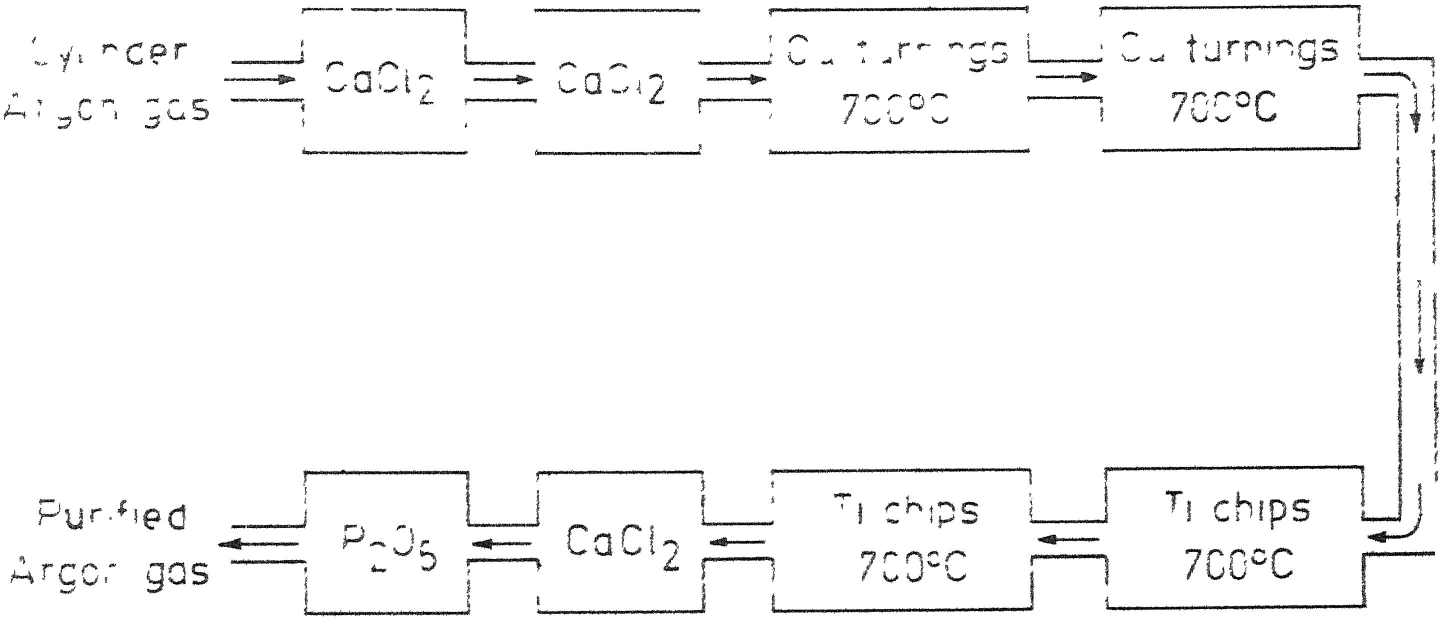

CK DIAGRAM REPRESENTING
PURIFICATION SYSTEM.

solubility of O_2), at the same time the reaction rate between oxygen and Cu turnings or Ti chips accelerated. Argon gas from the gas cylinder was passed through the $CaCl_2$ tubes to remove the bulk of the moisture and then through hot Cu turnings to remove O_2 and traces of H_2O. The gas was then passed through Ti chips to remove O_2, N_2 and H_2. The gas was finally passed through $CaCl_2$ and P_2O_5 to remove the last traces of moisture. This gas was used for flushing and final filling up of the arc furnace chamber.

Melting Procedure: The weighed materials were always charged in the copper crucible in a particular sequence so as to keep the evaporation losses the same and at the minimum. Mischmetal which is the lowest melting component (m.p. ~ 900°C) amongst the three components, Mm, Co and Fe, and has reasonable vapour pressure at 1 atm. pressure, was always kept at the bottom and was covered completely by iron and cobalt pieces. Thus, initially, the arc was always struck between the tungsten electrode and an iron piece kept at the top. Before each melting operation the furnace chamber was evacuated to about 20μ Hg pressure and flushed with purified argon gas from the gas purification system. This procedure was repeated 3 or 4 times to ensure removal of all the air from the furnace chamber. Finally, the furnace chamber was filled with purified argon gas. In the first melting, by setting the start and weld controls at 12 and 10 respectively, lower arc pressure was used to avoid sputtering of small pieces of material. The time was set at 20 secs to have a short melting time. But, in the subsequent meltings of the alloy button the start and weld controls were set at 18 and 15 respectively and the timer was set at 30 secs so that higher arc pressure and longer melting times could be used for proper homogenization of the material. Each alloy was melted 3 to 4 times and at each remelting the alloy button was put upside down so as to produce better homogenization. After melting, the alloy was weighed to find out the total loss. It was found that the maximum loss was less than 1 percent. Some of the alloys were chemically analysed for Fe and Co to check whether or not the alloys with compositions close to the intended one could be prepared.

For phase analysis of the alloys, the alloys had to be properly homogenized before they were subjected to x-ray diffraction and metallographic analysis. Since the alloys were rather reactive and each method of analysis was spread over several days it was necessary protect them from oxidation. For storage of the alloys till they were needed a vacuum desiccator kept at 750μ Hg pressure was used.

Annealing: The as cast samples were broken into pieces of suitable size and the surfaces of the pieces were ground to remove any oxide that might have formed during melting or storage. The alloys were sealed in evacuated quartz tubes at a pressure of 20×10^{-3} mm Hg. Sufficient space was left between the walls of the quartz tubes and the samples to avoid breakage of quartz tubes due to thermal expansion of the alloy pieces. Long pieces of an alloy were put, wherever possible, because the small pieces had a tendency to get stuck (mechanical jamming) in the quartz tubes leading to their breakage when heated. In a batch, five to six such quartz tubes containing different alloy samples were annealed and proper care was taken to identify them. In the beginning, the arc melted alloys were heat treated at a reasonably low temperature to see if any problem, like reaction with quartz tubes, oxidation in the residual air etc was encountered during annealing. Initial annealing was done in a vertical tube resistance furnace at $500^{\circ} \pm 1^{\circ}$C for 5 days. The alloys were quenched in tap water. No reaction between the quartz tubes and the alloys could be detected. Some of the alloys after their low temperature annealing showed three phases while the same samples showed only two phases after annealing at 900°C for 5 days indicating that the 5 day annealing at 500°C was not sufficient for homogenization. Subsequently, it was found that a 4 day anneal at 900°C (or higher time anneal at 900°C) produced the same microstructure of the alloys as that in a 5 day or a longer anneal. Hence, all alloys were annealed at 900°C for 4 days and finally quenched in tap water. The annealed alloys were also stored in the evacuated desiccator.

Metallographic Analysis: A small and representative portion of the annealed alloy was taken from the annealed sample for metallographic analysis. A vertical section from the melted button, which would show up any segregation or inhomogeneity of the phases, was generally selected for this purpose. The samples for metallography were mounted in lucite. The mounted samples were polished on 1/0 through 4/0 emery papers. Finally, the samples were polished on a wheel covered with microcloth using 0.5u alumina powder suspended in water as the abrasive. After polishing, the samples were thoroughly washed with water, rinsed with alcohol and dried under a high speed blower. The samples were checked under an optical microscope in the as-polished condition to detect the presence of inhomogeneities and oxides. The polished samples were then etched to reveal the microstructures. The etching reagent used (Nital) consisted of 2.5 ml. conc. HNO_3 in 97.5 ml of pure methanol. All the samples were etched to the same extent so that different samples processed in the same manner could be compared. After etching, the samples were thoroughly washed with water, rinsed with alcohol and dried under a blower. The concentration of the acid in the etchant and the etching time were varied for some of the samples to obtain better contrast among the phases. A 1 percent nital solution was found suitable for revealing three phases in some of the 3- phase alloys.

X-ray Diffraction Analysis: About 3 to 4 gms of the annealed sample was used for x-ray diffraction work. Most of the alloys were very brittle and so it was easy to prepare -300 mesh powder using steel and agate mortars and pestles. But, some of the high Fe alloys were found to be comparatively tough and grinding had to be continued till the whole material passed through the sieve. Since the diffraction patterns with the as-crushed powder produced sharp diffraction lines, the powders were not annealed before taking diffraction patterns.

For phase identification, the diffractometer patterns were obtained using a G.E. XRD-6 diffractometer with unfiltered Cr-radiation at 30 KV, 17 mA. The criterion used in choosing the diffractometer in comparision with the Debye-Scherrer technique and the radiation were : high resolution of the diffractometer, high resolution due to the long wave length of Cr-radiation and shorter time to obtain a diffraction pattern. All the diffraction patterns were obtained in the angular range of $30^\circ < 2\theta < 145^\circ$. The diffractometer conditions used in recording the diffraction patterns were scanning speed of 2^{o}/min, slit system 3^{o} MR MR / 0.2^{o}, time constant of 4.0, a range of 500 cps and a chart speed of 30"/hr. Unfiltered radiation was used so that the weak peaks could be detected. Some of the very weak peaks, however, could not be clearly seen in the diffractometer traces because of reasonably large noise in the recording system. For phase analysis the diffraction traces of pure or nearly pure phases were used as standard patterns for comparison with other diffraction traces. The diffraction patterns of pure or nearly pure phases were taken using a 114.6 mm dia Debye-Scherrer Camera. These diffraction patterns were used for proper identification, through indexing of the diffraction patterns, of phases. An exposure of 9 hrs. with unfiltered Cu-radiation at 30 KV and 15 mA gave good diffraction patterns. After the x-ray work was completed, the powdered samples were stored in evacuated and sealed pyrex glass tubes for future use.

III.2 Thermal Analysis:

For determining the melting points of RE-Co-Fe alloys, the thermal analysis apparatus described in Chapter II was used. Since the RE-Co alloys are reported to react with Al_2O_3 crucibles (50) special precautions were taken to avoid damage of the furnace assembly due to seepage of material through the crucible. Two concentric, sintered Al_2O_3 crucibles, instead of one, were used for keeping the material. Since the melting points of the investigated ternary alloys could not be guessed from the binary systems, for the first trial run an alloy with the lowest Fe was chosen. It was expected that its melting point would not be far from those shown by the binary diagrams. An available RE-Co-Fe two-phase (containing $RECo_5$ and RE_2Co_{17} type phases) alloy with least amount of Fe was chosen and it was kept in the locally made Al_2O_3 crucibles. After keeping the crucibles in the furnace, the furnace chamber was evacuated and flushed with argon gas 3 or 4 times. Since the thermocouple was to be protected with a thin Al_2O_3 sheath and it was not known how the thermocouple sheath would behave in the molten RE alloy, in the first run it was kept outside the melt. The furnace was heated up slowly and when the temperature reached about 1350°C (known from the applied voltage, see Appendix I) the thermocouple along with its protection sheath was pushed into the melt so as to start thermal analysis. But, this attempt was unsuccessful because the material in the crucible was found to be in partially molten condition. Later, a relatively pure $MM(Co,Fe)_5$ alloy close to the binary (which was expected to have lower melting temperature) was used for thermal analysis. This time, the thermocouple along with the Al_2O_3 sheath was kept inside the material from the beginning. Thermal analysis run was made following the procedure given in Chapter II.

III.3 Curie Temperature Measurement:

For determining the Curie temperatures of RE-Co-Fe alloys, an apparatus fabricated by R.C. Mittal (57) was used. It essentially consisted of a small nichrome-wound furnace kept in a vacuum chamber - a pyrex glass bell jar with a long tube at its top. A sealed end brass tube inserted into the furnace chamber through an 'O' ring joint could be moved up or down for lowering or raising the sample. The sample was kept in a quartz tube hung from the bottom end of the brass tube. For measuring the temperature, a thermocouple was inserted into the material through the brass tube, an alumina sheath was used for protecting the thermocouple. An induction coil kept over the long tube portion of the chamber was used for determining the flux change as a function of temperature. A differential method was adopted to measure small changes in induced voltage. A rectifier circuit with provision for continuous balancing of the rectified voltage to a near null voltage was used for converting the A.C. signal to a D.C. signal. The D.C. output voltage from the rectifier circuit was amplified using a D.C. microvolt amplifier with various D.C. ranges (0-100μV full scale to 0-1000 V full scale) and recorded on a Sargent strip chart recorder.

For determining the Curie temperatures of different phases as a function of amount of Fe, single phase, two phase as well as three phase alloys were used. The sample along with the silica sheath was kept in the quartz tube and the thermocouple was inserted into the silica sheath. After putting the properly cleaned 'O' rings in their respective positions, the chamber was evacuated ($\simeq 10^{-4}$ mm Hg pressure) using rotary and diffusion pumps. The sample was inserted into the furnace and was heated above its Curie temperature. It was then brought into the induction coil. The balancing circuit was quickly activated to get a near null voltage. Then, the voltage was recorded continuously on the recorder. The specimen temperature was read continuously with the help of a potentiometer and recorded on the strip chart recorder. The maximum inaccuracy of noting the temperature in this method was about 2° to 3°C. Three to four runs were made with each sample to check the reproducibility. For reasons described in the results section, a slightly different procedure was adopted in later runs. Before lowering the sample into the furnace, the furnace was heated upto 900°C (or 950°C if required), the same temperature at which the sample was annealed. Then the sample was lowered into the furnace. When the sample temperature reached 900°C, it was immediately pulled out and placed in the induction coil. The output voltage as well as the temperature were recorded on the sargent

CENTRAL LIBRARY
Acc. No. A 51149

recorder. Sufficient care was taken to prevent the vacuum chamber from getting heated up.

III.4 Magnetic Easy Axis Determination:

As has been pointed out in the introduction section, the easy axis of magnetization of $RECo_5$ and RE_2Co_{17} alloys are either along the crystallographic c-axis or in the basal plane. If the powdered samples consist of single domain particles, then in a small magnetic field the loose powders are expected to align themselves along the easy axis. In such oriented samples, the particles will arrange themselves with their easy axis along the direction of the magnetic field but will have random orientations around this easy axis. This aligned specimen is thus similar to a sample with wire texture. Hence, the oriented specimen diffraction pattern should show similar streaky pattern as is obtained with drawn wires or fibres. Thus the easy magnetisation axis can be determined in the same way as the wire axis is determined.

For preparing the oriented sample of alloy 51, a small amount of -300 mesh powder was taken on a card and a small $SmCo_5$ magnet was placed below the card. A little juggling of the magnet produced short thin magnetically aligned needles standing erect on the card. These needles were frozen in by spraying krylon clear plastic spray on them. The magnet was then removed and the needles were removed by scraping the paper with a sharp razor blade. Of the large number of needles produced, the thinnest and the most uniform one (determined by visual observation) was mounted in a 57.3 mm dia Weissenberg Camera and a powder pattern was recorded. The diffraction pattern obtained showed basically continuous Debye rings with indications that some of the diffraction lines have non-uniform intensity distribution. Since the alloy 51 was somewhat tough compared to some other alloys of higher RE content, it was thought that the surface layers of the particles might have got some plastic flow during the mechanical grinding operation causing apparent randomness and hence were producing continuous Debye rings. To remove the disturbed layers from the particle surface, the alloy powder was subsequently etched by 5 percent nital for 30 secs. The diffraction pattern obtained with the etched powder showed clear streaky pattern as is expected from a well aligned specimen. After locating the ideal position of the diffraction spots on the intensity streaks of the diffraction pattern, the position of the same spots on a flat film, kept at the same distance from the specimen as the cylindrical film, was determined by geometrical principles. Then the standard procedure for wire texture determination was adopted.

CHAPTER IV

RESULTS AND DISCUSSION

IV.1 Phase Equilibria:

Some of the rare earth elements present in Mischmetal have complete solid solubility whereas others have extended solubility among themselves (33). For an individual transition metal (Mn, Fe, Co or Ni), the binary systems with different rare earths exhibit similar binary phase equilibria. This is in general true also for the non-transition metal-rare earth binary systems. Hence, when rare earth elements are present together, as in Mischmetal, the phase equilibria is expected to be similar to that of the rare earth binary systems. The work of Fishman and Crowe (34) on the MM-Mg system indicate that this assumption is a reasonably good one. Assuming that the above observations are in general true, the MM-Co-Fe system can be represented as RE-Co-Fe system, where RE stands for the rare earth elements present in MM. The RE-Co-Fe system was studied in this investigation through metallographic as well as x-ray diffraction techniques. For phase analysis by x-ray diffraction, standard patterns of the $RECo_5$ and RE_2Co_{17} phases (57) were utilized. The phase analysis results of the 900°C annealed alloys are tabulated in Table IV.1. The isothermal section of the RE-Co-Fe system drawn on the basis of the above analysis is represented in Fig. IV.1. Some of the alloys were

TABLE IV.1

Phase Analysis of the RE-Co-Fe System

Alloy No.	Intended Composition of Alloy in at. pct. of			Phase Analysis	
	RE	Co	Fe	Metallography	X-ray Diffraction
8	16.66	63.34	20.0	3	RE_2Co_7+$RECo_5$+S
12	20.0	65.0	15.0	2	RE_2Co_7+$RECo_5$
14	20.0	60.0	20.0	3	RE_2Co_7+$RECo_5$+S
15	16.0	64.0	20.0	3	RE_2Co_7+$RECo_5$+S
16	15.0	60.0	25.0	2	RE_2Co_7+S
17	15.0	55.0	30.0	2	RE_2Co_7+S+A
18	15.0	50.0	35.0	2	S+A
19	15.0	45.0	40.0	2	S+A
22	17.0	43.0	40.0	2	S+A
23	13.5	46.5	40.0	2	S+A
25	14.0	56.0	30.0	2	RE_2Co_7+S+A
28	12.75	47.25	40.0	2	S+A
30	15.0	65.0	20.0	3	RE_2Co_7+$RECo_5$+S
31	11.75	38.25	50.0	2	S+X
33	18.0	35.5	46.5	2	A+Y
34	17.5	32.5	50.0	2	A+Y
35	11.0	34.0	55.0	2	S+T+X
39	13.0	52.0	35.0	2	S+A
41	12.11	62.33	25.54	2	S+A
42	18.0	42.0	40.0	2	S+A
43	16.5	33.5	50.0	2	S+A
47	12.5	52.5	35.0	2	S+A
48	13.5	61.5	25.0	2	S+A
50	12.75	62.25	25.0	2	S+A
51	12.0	53.0	35.0	2	S+A
52	19.0	51.0	30.0	2	RE_2Co_7+A
53	16.5	28.5	55.0	2	T+Z

chemically analysed. The intended and analysed compositions shown in Table IV.2 indicate that the losses are small. Since the analysed compositions are very close to the intended ones, the phase equilibria shown in Fig. IV.1 has been drawn on the basis of the intended compositions of alloys.

In Figure IV.1 several dash dot lines are drawn along certain constant RE contents to represent the hypothetical A_xB_y quasi-binaries corresponding to the high cobalt RE-Co phases. Of these quasi-binary lines, the AB_2 and A_2B_{17} lines are drawn between the RE-Co and RE-Fe binaries because in both these systems the AB_2 and A_2B_{17} type phases exist and extension of these phases from one binary to the other may exist along these lines. On the other hand, the other A_xB_y lines are drawn only upto the middle of the ternary diagram (these A_xB_y compounds are not found in the RE-Fe system) to indicate that these A_xB_y phases may extend to some extent along these lines. In this investigation only a part of the RE-Co-Fe system was studied. In the investigated region of the RE-Co-Fe system, besides the A_2B_{17} type phase two new phases, A-phase and S-phase, were found to exist. Among the investigated alloys, only two alloys, alloy 12 with 15 at. pct. Fe and alloy 14 with 20 at. pct. Fe, were found to have the RE_2Co_7 type phase as the major phase; the alloy 14 was found to have three phases (Fig. IV.2) whereas the alloy 12 was

TABLE IV.2

Chemical Analysis of Several RE-Co-Fe Alloys

Alloy No.	Composition, wt percent			
	Intended		Analyzed	
	Fe	Co	Fe	Co
30	15.84	54.34	15.3	54.0
35	46.42	30.29	46.2	30.1
41	20.99	54.04	20.8	53.4

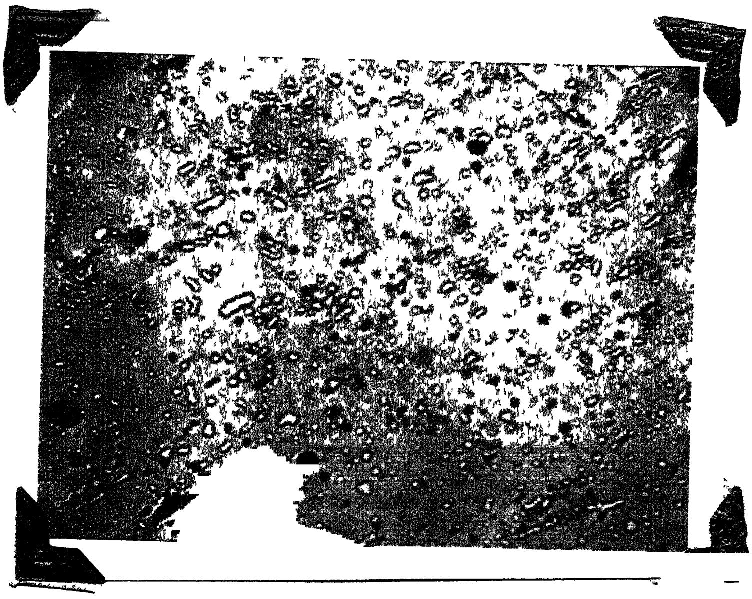

Fig. IV.2 Microstructure of Alloy 14 (200 X)
Photograph shows only two phases; RE_2Co_7-type phase (dark matrix) and $RECo_5$ type phase (bright second phase)

having only two phases. The second and third phases in these alloys were in very small amounts and hence these alloys could be considered as boundary alloys. Since the RE_2Co_7 phase exists in the RE-Co system of Ce, La and Nd, the three major components of MM, it is expected that the MM_2Co_7 phase exists. The RE_2Co_7 type phase at low Fe concentrations was not studied. From the phase analysis of the RE-Co-Fe alloys, it appears that the RE_2Co_7 type phase extends from the RE-Co binary upto at least about 20 at. pct. Fe. One characteristic feature of the extension of the RE_2Co_7 phase into the ternary is that the phase region deviates from the hypothetical A_2B_{17} line towards higher (Co,Fe) side. While no data on the phase extension of the A_2B_7 type phase is available in the literature, some observations have been made with respect to AB_5 compounds. Buschow (30) and Taylor and Poldy (58) could not produce single phase samples of $RE(Co_{1-x}Fe_x)_5$, where RE = Sm or Y, with larger amounts of Fe (> 5 percent) unless the stoichiometry was allowed to shift towards higher (Co,Fe) side.

The S-phase appears to be stable over a reasonably wide Fe concentrations. The lowest and highest Fe contents in the S-phase were estimated through the microstructure and x-ray diffraction analysis. The x-ray diffraction patterns of alloys 8,14,15 and 30 showed diffraction lines due to the

RE_2Co_7, $RECo_5$ and S phases. On metallographic analysis, the same alloys revealed two phases when 2.5 percent Nital was used but on using 1 percent Nital three phases could be clearly seen (Fig. IV.3). Colouration produced on one of the phases masked the third phase when 2.5 percent Nital was used. The alloys 8 and 14, out of the four three phase alloys, contained the third phase $RECo_5$ in quite small amounts indicating that these alloys were close to one side of the three phase triangle. In an attempt to draw the three phase triangle, it was found that the three phase corner at the S-phase is near about 21 at. pct. Fe. Thus, the lower Fe limit of the S-phase is possibly at 21 at. pct Fe or is at a somewhat lower Fe concentration. At the higher Fe side of the S-phase the alloy 31 has two phases, the amount of second phase being very small (Fig. IV.4). The x-ray diffraction pattern of alloy 31 showed the S-phase lines together with a few weak lines possibly due to the second phase. The alloy 35 also showed two phases, the second phase was in small amounts and looked the same as the second phase in alloy 31. The diffraction pattern of alloy 35, however, indicated that besides all the lines present in alloy 31, there were some weak lines and that the relative intensity relations of the S phase lines were not quite the same as in alloy 31 or alloy 51 diffraction patterns. This indicated that the alloy 35 had three phases - the S phase, the X phase, to the higher (Co,Fe) side of the S phase, and

Fig. IV.3 Microstructure of Alloy 15 (1000 X).
Photograph shows three phases; RE_2Co_7-type phase (dark matrix), S phase (bright second phase) and $RECo_5$ type phase (bright needle like structure) which is in very small amount.

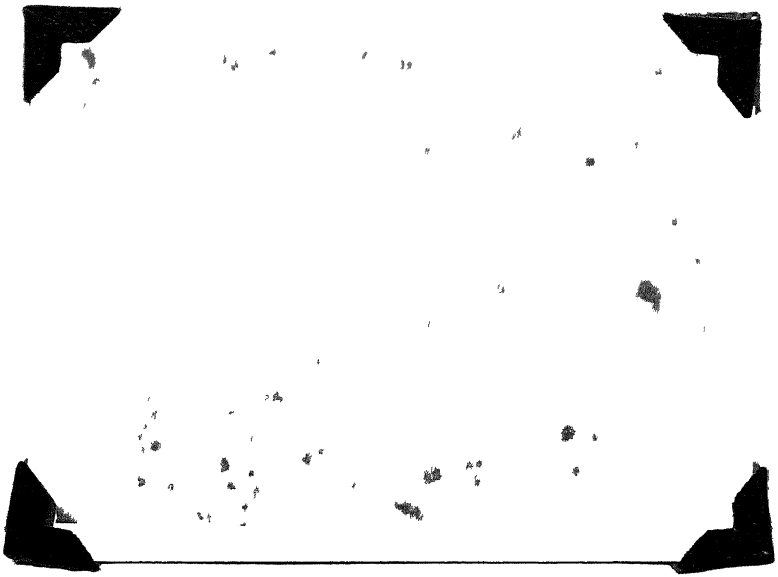

Fig. IV.4 Microstructure of Alloy 31 (200 X)
Photograph shows two phases; S phase (matrix) and X phase (bright) in small amounts.

the T phase, possibly at a higher Fe content. The x-ray and metallographic observations on alloy 35 indicate that the S phase possibly extends to a Fe content less than 55 at. pct. Fe. Tentatively, this limit has been shown in Fig. IV.1 as about 51 at. pct. Fe. Metallographic observations on alloy 51 (Fig. IV.5) and alloy 31 indicate that the S-phase region is rather narrow. It is known from the literature that the RE_2Co_{17} phase extends from the RE-Co system to the RE_2Fe_{17} phase in the RE-Fe binary (59). The S-phase extends almost parallel to the A_2B_{17} line and is very close to it. This indicates that the extension of the RE_2Co_{17} type phase must be to the higher (Co,Fe) side of the A_2B_{17} line. It is possible that the x phase is the RE_2Co_{17} type phase. The unidentified diffraction lines in the diffraction patterns of alloy 31 and alloy 35 were too few to identify the x phase as the RE_2Co_{17} type phase. The A phase was found to extend along the same direction of the extension as the RE_2Co_7 type phase. Alloy 52 showed two phases, almost in equal amounts, in the microstructure (Fig. IV.6) and the diffraction pattern showed the diffraction lines due to the A and RE_2Co_7 type phases. The position of alloy 52 relative to the RE_2Co_7 type phase and the A phase indicates that the A phase region extends at least down to about 35 at. pct. Fe and the RE_2Co_7 type phase extends at least upto 25 at. pct. Fe. Alloy 53

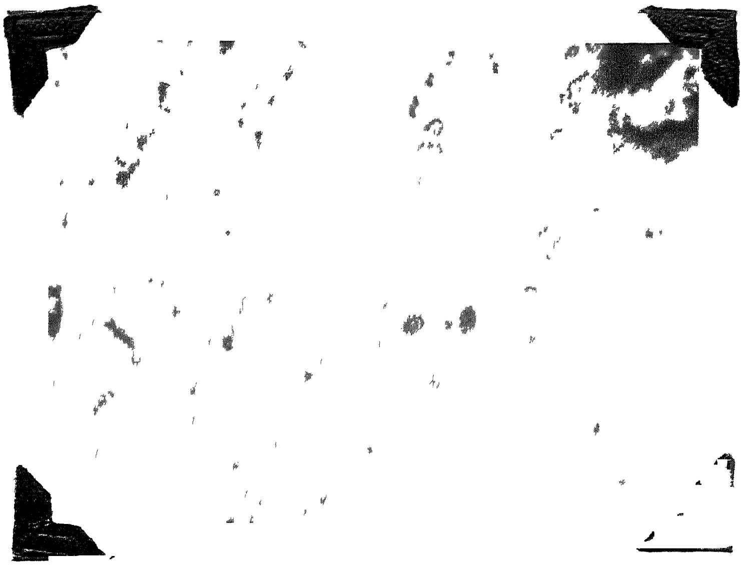

Fig. IV.5 Microstructure of Alloy 51 (400 X)
Photograph shows two phases; S phase (matrix)
and A phase (dark second phase) in small amou

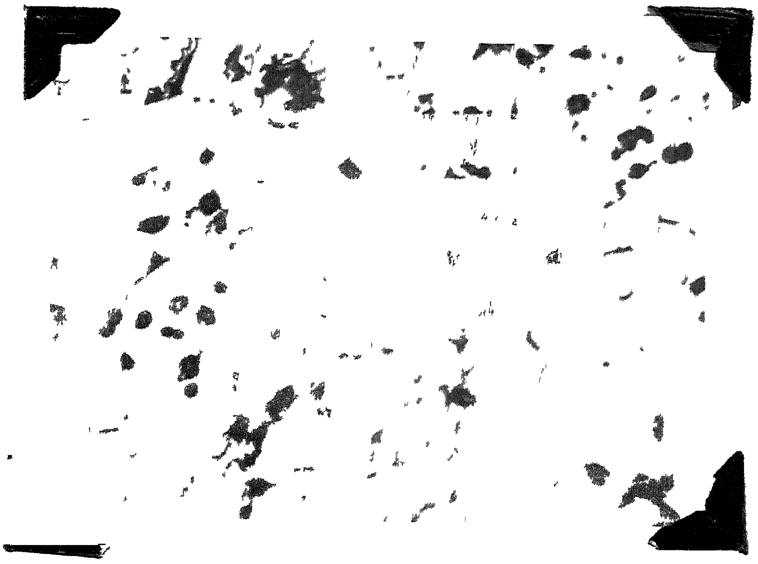

Fig. IV.6 Microstructure of Alloy 52 (400 X)
Photograph shows two phases; RE$_2$Co$_7$ type pha
and A phase (bright second phase)

at 55 at. pct. Fe was found to have two phases, none of which resembled the A or S phases. The diffraction pattern showed lines which matched with the T phase lines observed in alloy 35. This indicates that the alloy 53 possibly has the T phase and a phase (Z phase), with higher RE content than the A phase. Since the alloy 53 has two phases, a three phase region between alloy 53 and A phase is expected. On this basis, the extension of the A phase region to higher Fe side has been shown to be about 53 at. pct. Fe. Alloy 34 showed two phases in the microstructure (Fig. IV.7) and the diffraction pattern showed the diffraction lines due to the A phase and another phase, y phase, possibly a phase with higher RE content than the A phase. Alloy 42 showed two phases in the microstructure (Fig. IV.8) and the diffraction pattern showed the diffraction lines due to the A and S phases. The microstructures of alloys 34 and 42 clearly showed that the second phases in these alloys were different. Thus, alloy 42 and alloy 34 are on either side of the A phase. A comparison of their compositions indicates that the A phase region is rather narrow. With increase in Fe content the A phase region was found to extend towards higher (Co,Fe) side and at about 52 at. pct. Fe it crossed the AB_5 line. This composition will be useful in determining the crystal structure of the A phase.

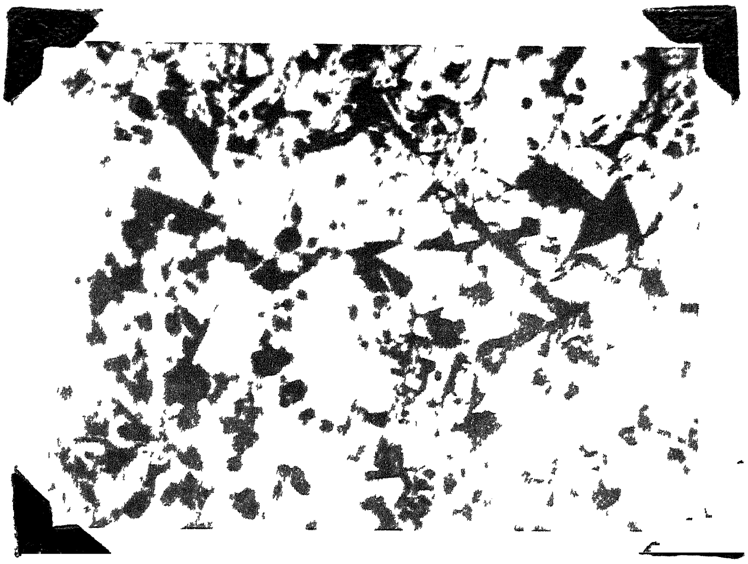

Fig. IV.7 Microstructure of Alloy 34 (200 X)
Photograph shows two phases; Bright A phase and dark Y phase. Black spots are probably pits.

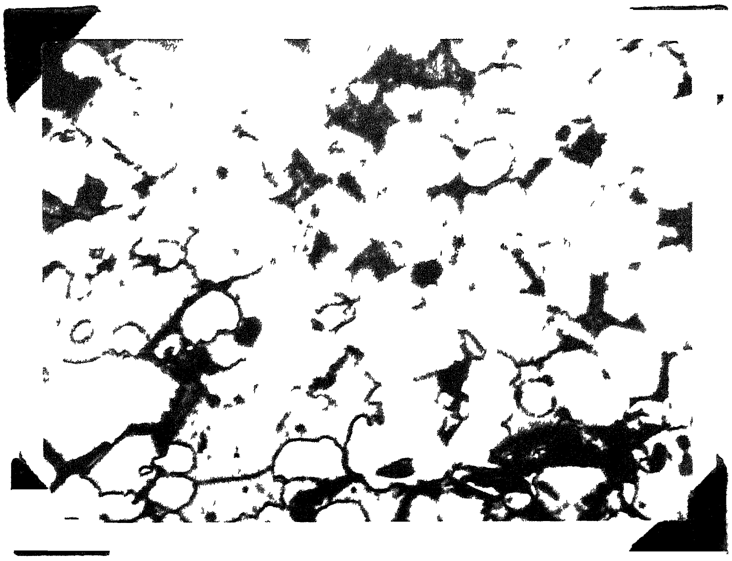

Fig. IV.8 Microstructure of Alloy 42 (400 X)
Photograph shows two phases; A phase (dark matrix) and S phase (bright).

Alloys 17 and 25 were found to have two phases in microstructure but their x-ray diffraction patterns revealed the presence of A, S and RE_2Co_7 type phases. It is possible that like in alloy 35, the three phases are not revealed by the etching reagent used. On the basis of the x-ray diffraction data these alloys are shown within a three phase triangle drawn between A, S and RE_2Co_7 phases.

The diffraction patterns of S and A phases are very similar to that of the RE_2Co_{17} phase. For easy comparison, the diffraction patterns of A, S and RE_2Co_{17} phases are shown in Fig. IV.9 in a modified manner. The diffraction peak positions are shown as vertical lines drawn at the appropriate 2θ values, the height of the lines represents the relative intensities of various diffraction lines. The diffraction peaks of the A, S and RE_2Co_{17} phases in the low angle region of the diffraction pattern overlap considerably and cause difficulty in identification of the three phases if present together. The diffraction peaks in the high angle region of the diffraction pattern are relatively widely spaced and for phase identification these peaks have been found valuable.

Since the diffraction patterns of the A and S phases resemble that of the RE_2Co_{17} phase, an attempt was made to index these diffraction patterns with the help of the RE_2Co_{17}

gonal
s of
th
RE
re
cach
$\bar{1}$ 10]
gonal
s

asal
when
etry
y
k
of
mbo-
es
g in
tep

y of
th
a

structure. A characteristic feature of the RE_2Co_{17} hexagonal structure (Fig. IV.10) is that it can be thought in terms of stacking of blocks consisting of two atom layers, one with a layer of Co atoms only and the other, a mixed layer of RE and Co atoms. Hexagonal or rhombohedral RE_2Co_{17} structure can be generated by stacking these blocks after shifting each block with respect to the other through a distance 1/3 [$\bar{1}$ 10] (Fig. IV.11). The sequence **ab ab....** generates the hexagonal RE_2Co_{17} structure and the sequence **abc abc....** generates the rhombohedral RE_2Co_{17} structure (Fig. IV.12). One important feature of such layer structures is that the basal plane dimensions, i.e., the a parameters, do not change when the structure changes from hexagonal to rhombohedral symmetry (eg. a parameter of α- and β-Ce_2Co_{17} are same (15)), only the c parameter changes due to addition of one more block in the rhombohedral structure. The diffraction patterns of the A and S phases being quite similar to that of the rhombohedral RE_2Co_{17} phase, the structures of the A and S phases may be obtained through proper stacking of blocks, keeping in mind the stoichiometry of the phases. As a preliminary step towards determining the structure of these phases, the diffraction patterns were tried to be indexed. Since many of the diffraction lines of the A and S phases match well with those of the RE_2Co_{17} structure, an estimate of the c and a

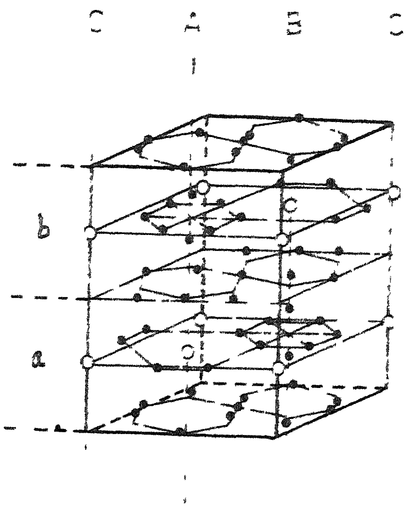

FIG IV 10 HEXAGONAL Th_2Ni_{17} STRUCTURE (62)

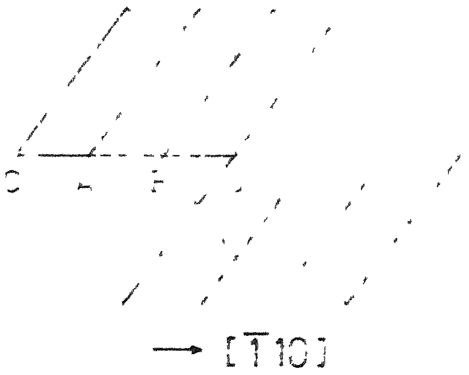

FIG IV 11 SCHEMATIC REPRESENTATION OF STACKING OF BLOCKS IN Th_2Zn_{17} STRUCTUR

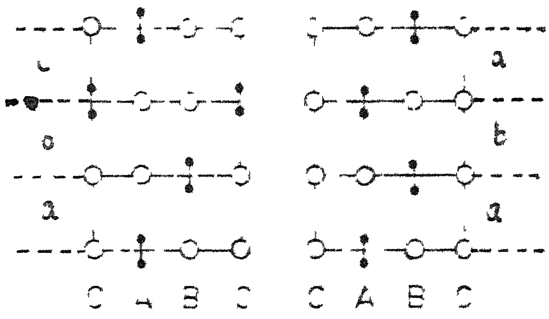

Th_2Zn_{17} IDEAL Th_2Ni_{17}

FIG. IV 12 SCHEMATIC REPRESENTATION OF Th_2Zn_{17}-TYPE AND Th_2Ni_{17}-TYPE STRUCTURES (60) parameters was made using the hkl indices of these lines on the basis of the rhombohedral RE_2Co_{17} structure. Since in the rhombohedral RE_2Co_{17} structure there are three blocks, height of each block can be calculated from the determined c parameter. Assuming that the S and A phases are multi-block structures, the c/a values for structures having upto eight stacks of blocks were calculated. Indexing of the diffraction patterns of the two phases was tried with a Bunn chart at these pre-determined c/a values. The most probable lattice was determined in each case by comparing the observed d values with the d values calculated on the basis of indexing. For the A and S phases, the indexed patterns are shown in Tables IV.3 and IV.4.

The diffraction pattern of the A phase (alloy 42) could be indexed on the basis of a hexagonal cell with lattice parameters, a = 8.495 A°, c = 22.663 A° and c/a = 2.668, corresponding to a stacking of 5½ blocks. The indexed pattern of alloy 42 is shown in Table IV.3. The diffraction pattern of the S phase (alloy 51) could be indexed on the basis of a hexagonal cell with lattice parameters, a = 8.551 A°, c=12.405 A° and c/a = 1.45, corresponding to a stacking of 3 blocks. The indexed pattern of alloy 51 is shown in Table IV.4. The lattice parameter of the S phase is the same as the corresponding RE_2Co_{17} phase. However, there are extra

TABLE IV.3

X-ray Diffraction Pattern of the A-phase

Hexagonal Cell - a = 8.495 Å, c = 22.663 Å and c/a = 2.668

Line No.	Relative Intensity	h k l	$d_{observed}$	$d_{calculated}$
1	VW	202	3.495	3.499
2	VW	007	3.252	3.238
3	VVW	204	3.060	3.085
4	M	107	2.962	2.963
5	VW	205	2.853	2.856
6	VW	116	2.805	2.823
7	M	211	2.743	2.760
8	VW	212	2.679	2.701
9	S	009	2.520	2.518
10	S	300	2.447	2.452
11	M	215	2.373	2.370
12	VW	00,10	2.267	2.266
13	W	10,10	2.176	2.166
14	VS	305	2.152	2.157
15	VS	220	2.123	2.124
16	VVS	217	2.107	2.109
17	VS	209	2.072	2.078
18	S	00,11;306	2.058	2.060;2.057
19	W	11,10	1.999	1.999
20	VS	00,12	1.890	1.890

TABLE IV.3 (contd)

Line No.	Relative Intensity	h k l	$d_{observed}$	$d_{calculated}$
21	VW	219;315	1.862	1.866;1.860
22	VW	308	1.858	1.854
23	VVW	229	1.630	1.624
24	VVW	410;411	1.603	1.606;1.601
25	VW	319;325	1.584	1.585;1.582
26	M	30,12	1.496	1.496
27	M	20,14	1.482	1.482
28	VW	502	1.457	1.459
29	VW	417	1.436	1.438
30	VVW	00,16;330	1.416	1.4164;1.4159
31	VVW	418	1.397	1.397
32	VVW	422	1.381	1.380
33	W	334	1.375	1.374
34	W	507	1.341	1.340
35	VVW	00,17^{x}	1.333	1.333
36	VVW	336;31,13	1.325	1.326;1.325
37	VW	40,12	1.317	1.318
38	W	11,17;509	1.271	1.272;1.270
39	W	40,13	1.265	1.265
40	S	30,16	1.228	1.227
41	S	600^{x}	1.226	1.226
42	W	602	1.218	1.219

TABLE IV.3 (contd.)

Line No.	Relative Intensity	h k l	$d_{observed}$	$d_{calculated}$
43	W	429;40,14	1.216	1.217;1.215
44	S	431;11,18	1.207	1.208;1.207
45	W	20,18	1.190	1.191
46	VW	22,16	1.1786	1.1784
47	VW	32,14;40,15	1.1678	1.1683;1.1675
48	W	50,12	1.1616	1.1607

[x] These lines were used for calculation of lattice parameters.

TABLE IV.4

X-ray Diffraction Pattern of the S-phase
Hexagonal cell - a = 8.551 Å , c = 12.4045 Å and c/a = 1.451

Line No.	Relative Intensity	h k l	$d_{observed}$	$d_{calculated}$
1	VW	201	3.538	3.549
2	VW	x	3.255	-
3	VW	202	3.164	3.180
4	S	113	2.972	2.973
5	W	104	2.869	2.862
6	VW	210	2.810	2.799
7	VW	211	2.717	2.731
8	VVW	x	2.618	-
9	VW	x	2.540	-
10	VS	300	2.462	2.469
11	S	204	2.381	2.379
12	VW	x	2.192	-
13	VS	220	2.137	2.138
14	VVS	303	2.122	2.120
15	VS	214	2.084	2.079
16	M	205	2.074	2.062
17	VW	222	2.019	2.021
18	VW	106	1.988	1.993
19	VW	312	1.945	1.950
20	VS	223	1.901	1.899
21	W	116	1.871	1.862
22	W	215	1.865	1.857
23	VW	401	1.829	1.831
24	VVW	402;007	1.773	1.774;1.773
25	VVW	107	1.725	1.724
26	VW	321;216	1.674	1.683;1.664
27	VW	117	1.647	1.638
28	W	322	1.631	1.639
29	W	315;306	1.583	1.583;1.586

TABLE IV.4 (contd.)

Line No.	Relative Intensity	h k l	$d_{observed}$	$d_{calculated}$
30	S	324	1.493	1.490
31	S	500	1.480	1.481
32	VW	331	1.413	1.416
33	VW	503;421	1.393	1.395;1.391
34	VW	227	1.370	1.365
35	VVW	218;109	1.358	1.357;1.356
36	M	317	1.339	1.342
37	VW	510	1.330	1.330
38	W	326[x]	1.313	1.313
39	VW	209	1.291	1.292
40	M	505	1.269	1.272
41	VS	601;327	1.227	1.228;1.227
42	S	514;10,10	1.223	1.223;1.224
43	W	431	1.216	1.212
44	W	602	1.213	1.211
45	VS	309[x]	1.203	1.204
46	W	520	1.186	1.186
47	VW	20,10	1.177	1.177
48	VW	522	1.166	1.165
49	VW	229	1.157	1.159

---

[x] These lines were used for calculation of lattice parameters

[xx] These lines could not be indexed. They are possibly due to impurities like oxides.

diffraction lines in the S phase pattern which indicate that the atomic ordering in this case is different than in the RE_2Co_{17} structure. No attempt was made to determine the complete crystal structure of these phases.

The diffraction pattern of RE_2Co_7 phase (alloy 12) has been indexed on the basis of a hexagonal Ce_2Ni_7 type structure with a = 4.974 A°, c = 24.948 A° and c/a = 5.007. The indexed pattern of alloy 12 is shown in Table IV.5. All the diffraction lines, however, could not be indexed; there are about five diffraction lines (weak and very weak lines) which could not be indexed. These lines are not due to the other phase present in alloy 12 viz, the $RECo_5$ phase. They may possibly be due to impurities like oxides.

Since for all the phases no single phase alloy was available, for determining lattice parameters of the A and S phases as a function of Fe content, two phase alloys with the least amount of second phase were chosen. With the help of two high angle reflections of each phase, the lattice parameters of the two phases were calculated. The calculated lattice parameters of the A and S phase alloys are tabulated in Tables IV.6(a) and (b) and are shown in Figs. IV.13(a) and (b) as a function of iron content of the alloys. As shown in the figure, the lattice parameters of the A phase alloys are practically unaffected by the addition of Fe. In the case

TABLE IV.5

X-ray Diffraction Pattern of the A_2B_7 - Type Phase (alloy - 12)

(Hexagonal Ce_2Ni_7 - type structure)

a = 4.974 Å c = 24.948 Å c/a = 5.016

Line No.	Relative Intensity	h k l	$d_{observed}$	$d_{calculated}$
1	VW	008	3.070	3.111
2	W	106	2.986	2.996
3	W	x	2.813	-
4	VS	107	2.735	2.748
5	W	x	2.657	-
6	VS	108	2.525	2.527
7	VVW	00,10	2.496	2.502
8	VVW	110	2.478	2.489
9	VW	112	2.455	2.453
10	VW	x	2.440	-
11	VVW	109	2.333	2.331
12	W	114	2.313	2.321
13	VW	00,11	2.258	2.262
14	VS	10,10	2.179	2.159
15	VVS	201	2.148	2.158
16	VW	202	2.126	2.134
17	W	x	2.110	-
18	VW	00,12	2.065	2.074
19	S	204	2.043	2.046
20	M	10,11	1.997	2.005
21	W	205	1.988	1.987
22	VW	118	1.948	1.949
23	VW	x	1.929	-
24	VVW	10,12	1.890	1.870
25	VVW	207	1.854	1.850
26	VW	11,10	1.759	1.764

TABLE IV.5 (contd.)

Line No.	Relative Intensity	h k l	$d_{observed}$	$d_{calculated}$
27	W	10,13	1.751	1.751
28	VVW	10,14	1.641	1.645
29	VVW	212	1.626	1.624
30	VVW	213	1.589	1.607
31	VVW	11,12	1.585	1.596
32	VVW	214	1.579	1.584
33	VW	00,16	1.532	1.555
34	M	20,12	1.494	1.498
35	W	10,16	1.458	1.464
36	VVW	11,14	1.447	1.449
37	M	300	1.439	1.444
38	M	302	1.428	1.435
39	M	20,13	1.426	1.434
40	VW	219	1.413	1.409
41	VW	304-	1.408	1.407
42	S	20,14[x̄]	1.373	1.373
43	S	21,10	1.370	1.368
44	VW	21,11	1.327	1.326
45	VW	20,15	1.315	1.317
46	VW	308-	1.310	1.310
47	VS	20,16[x̄]	1.263	1.263

---

[x] These lines could not be indexed. They may be due to impurities like oxides.

[x̄] These lines were used for calculation of lattice parameters

Note:- Key to symbols used in the Tables

VVW : Very Very Weak　S : Strong　VW : Very Weak

VS : Very Strong　W : Weak　VVS : Very Very Strong

M: Medium

TABLE IV.6

Lattice Parameters of S and A phases in the RE-Co-Fe System

Alloy No.	Intended at. pct. Fe	a (Å)	c (Å)	c/a
(a) A-phase				
42	40.0	8.50	22.77	2.68
33	46.5	8.50	22.77	2.68
34	50.0	8.50	22.77	2.68
(b) S-phase				
41	25.54	8.528	12.299	1.44
25	30.0	8.547	12.340	1.44
51	35.0	8.553	12.351	1.44
28	40.0	8.565	12.360	1.44
31	50.0	8.572	12.365	1.44

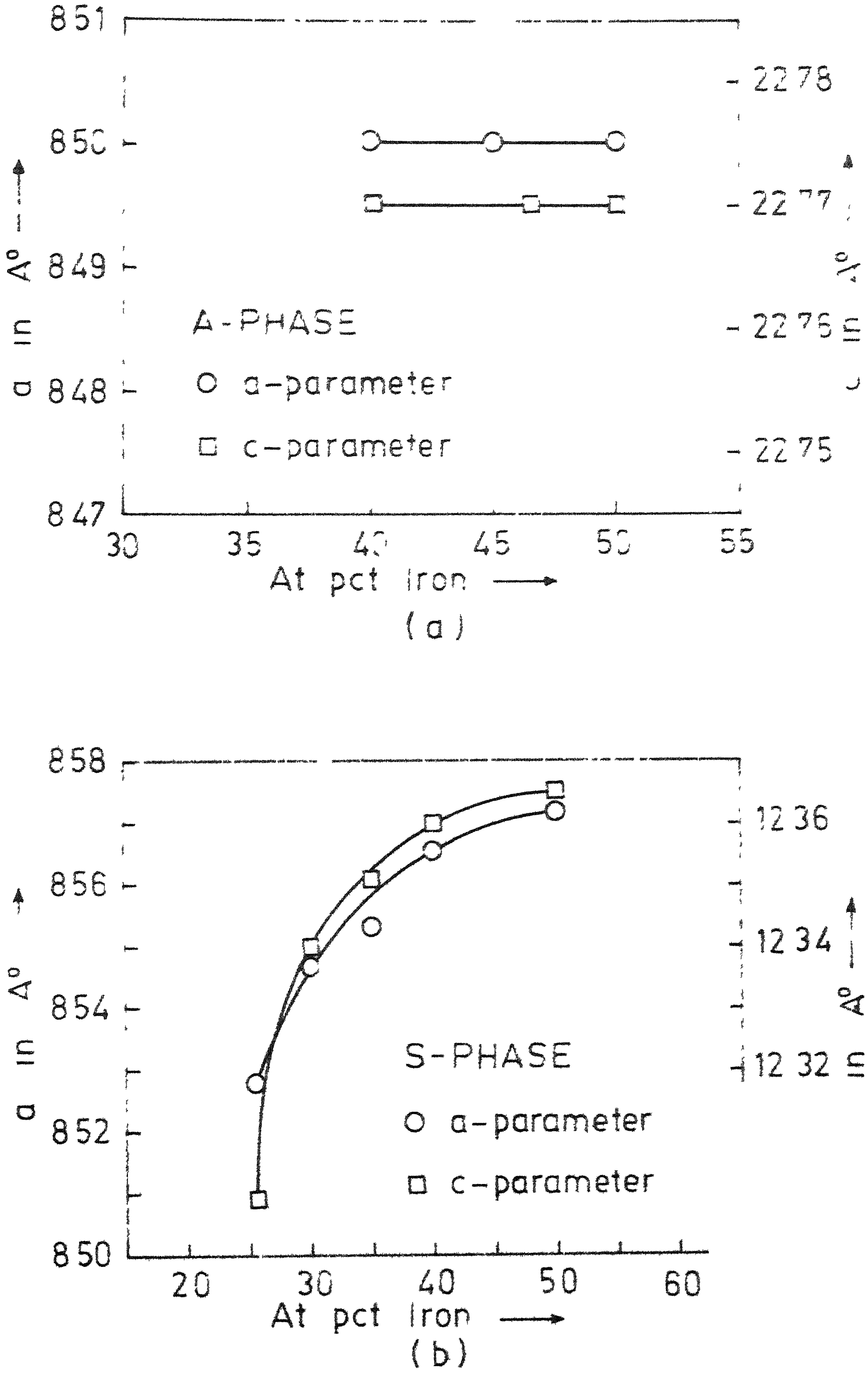

FIG.IV.13.LATTICE PARAMETERS OF I
PHAS .-PHASE (b) S

of the S phase, both the a and c parameters are found to increase with addition of Fe. As mentioned above, the S phase extends in a direction almost parallel to the A_2B_{17} line. Thus, the total RE content in the S phase alloys remains almost the same and the added iron is, then expected to replace the cobalt atoms in the S phase structure. Since the atomic radius of iron is not much different from that of cobalt (CN 12 atomic radii are being compared), the change in a and c parameters with replacement of Co by Fe is expected to be small. Contrary to the expected behaviour the lattice parameter data of the S phase in Fig. IV.13(b) indicate a large variation in c and a parameters with increase in Fe content; the increase being more for c than for a. Similar observations have been reported for the $RE_2(Co.Fe)_{17}$ phases by Ray et al (59). These authors explained the abnormal c-axis expansion in terms of the combined effects of increased magnetic ordering temperatures of the RE_2Fe_{17} phases conferred by the addition of Co and negative exchange interactions between certain atoms in the structures. In the present case the S phase structure is not known and whether a similar explanation for the change in lattice parameter of the S phase is applicable or not is not known. In the case of the A phase, the added Fe is expected to replace partially the RE atoms because the RE content decreases with increase in Fe content. Since the atomic radius of Fe is substantially less than that of RE it is expected that the A phase lattice should contract as Fe is added. It is possible, however, that Fe replaces RE in pairs as in the A_2B_{17} compounds. In that case increase in c parameter is expected. Contrary to these expectations, the c and a parameters of the A phase remain unaffected on addition of Fe. In the absence of detailed structural investigations, it is difficult to explain the lattice parameter variations of the S and A phases.

IV.2 Easy Axis of Magnetization:

In the present investigation, the easy axis of magnetization was determined by using a magnetically aligned needle of powder material and a Weissenberg camera. In taking a powder pattern with the needle formed from alloy 51 powder it was found that a good pattern, showing the streaks corresponding to preferred orientations caused by magnetic alignment of powder particles, could be obtained when the powder was etched with Nital to remove the disturbed surface layers. A similar observation has been reported for the $Sm_2(Co,Fe)_{17}$ alloys by Sergeyev et al. (61). These authors could improve the coercivity of the $Sm_2(Co,Fe)_{17}$ alloy powder by removing the disturbed layers from the particle surfaces by etching the powder with citric acid. The easy axis of magnetization for the etched powder of alloy 51 was found to be along the c-axis. For the other S phase alloys the easy axis has not been determined. In the literature it has been mentioned that the addition of about 10 percent iron to the MM_2Co_{17} phase changes the easy magnetization axis from basal plane to c-axis (Fig. I.9) and this c-axis magnetic symmetry is maintained upto about 50 percent Fe (27). The earlier investigators, however, are not clear in stating the exact compositions of the alloys chosen. It appears from their report that the alloys used were along the A_2B_{17} line. It this is the case, it is possible that these authors failed to distinguish between the A_2B_{17} and the S phases. The S phase region is very close to and is almost parallel to the A_2B_{17} line. It extends from somewhere around 20 at. pct. Fe to about 50 at. pct. Fe which closely agrees with the composition range in which the c-axis magnetic symmetry has been observed in the MM-Co-Fe phase. Thus, it appears that the magnetic symmetry change is not because of Fe addition in A_2B_{17} structure but due to formation of a new phase. If this is true, then the $RE_2(Co,Fe)_{17}$ phase, which appears to have deviated to the higher (Co,Fe) side, should continue to show basal plane magnetic symmetry between the RE_2Co_{17} and RE_2Fe_{17} compositions.

IV.3 Curie Temperature:

Induction method was adopted for determining the Curie temperatures (T_c) of the RE-Co-Fe alloys. In the initial runs when the sample was kept inside the furnace from the beginning (i.e. during heating up of the furnace) variation in Curie temperature was observed when the same specimen was cycled several times through the Curie temperature. This indicated that the material was undergoing some transformation. To reduce the extent of transformation, the material was kept at the high temperatures for the minimum time possible. To achieve this, the furnace was first heated upto 900°C (or 950°C), the temperature at which the alloys were initially annealed, and then the specimen was lowered into the furnace to heat it upto 900°C or 950°C. On reaching the temperature the specimen was drawn into the induction coil and allowed to cool. Several traces obtained with the alloys containing different phases are shown in Figs. IV.14 to IV.17. As shown in the figures, the RE$_2$Co$_{17}$, A and S phase alloys registered clear increase in induced voltages at the Curie temperatures. But, in the case of the RE$_2$Co$_7$ alloys large fluctuations in the induced voltage were observed. In the case of alloy 50 a three phase (RE$_2$Co$_7$+RECo$_5$+S) alloy, two peaks in the induced voltage vs temperature traces were observed as shown in Fig. IV.16. The two temperatures correspond to the S and RECo$_5$ phases. The change in induced voltage due to Curie temperature of the RE$_2$Co$_7$ phase could not be seen clearly; a small break in the trace at about 715°C (the approximate Curie temperature of the RE$_2$Co$_7$ phase) was, however, observed. This is possibly because of the presence of only small amount

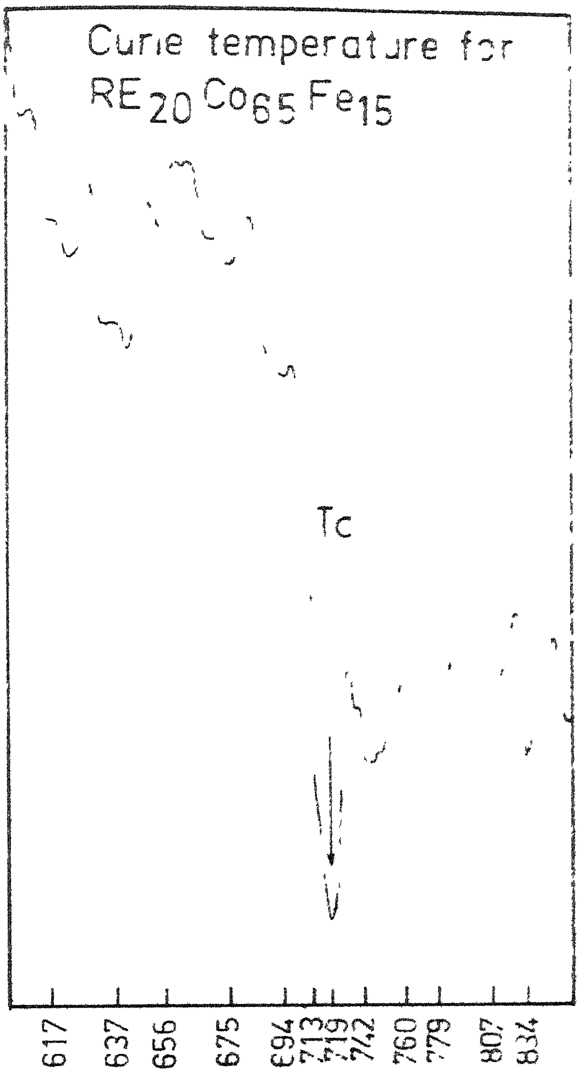

FIG IV 14 CURIE TEMPERATURE PLOT FOR RE$_2$Co$_7$ PHASE

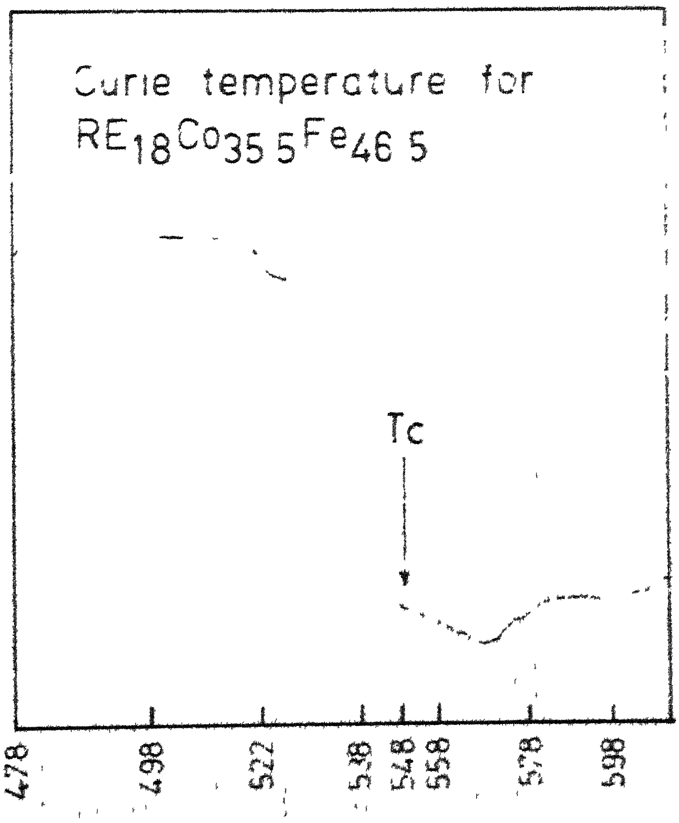

FIG IV 15. CURIE TEMPERATURE PLOT FOR A-PHASE

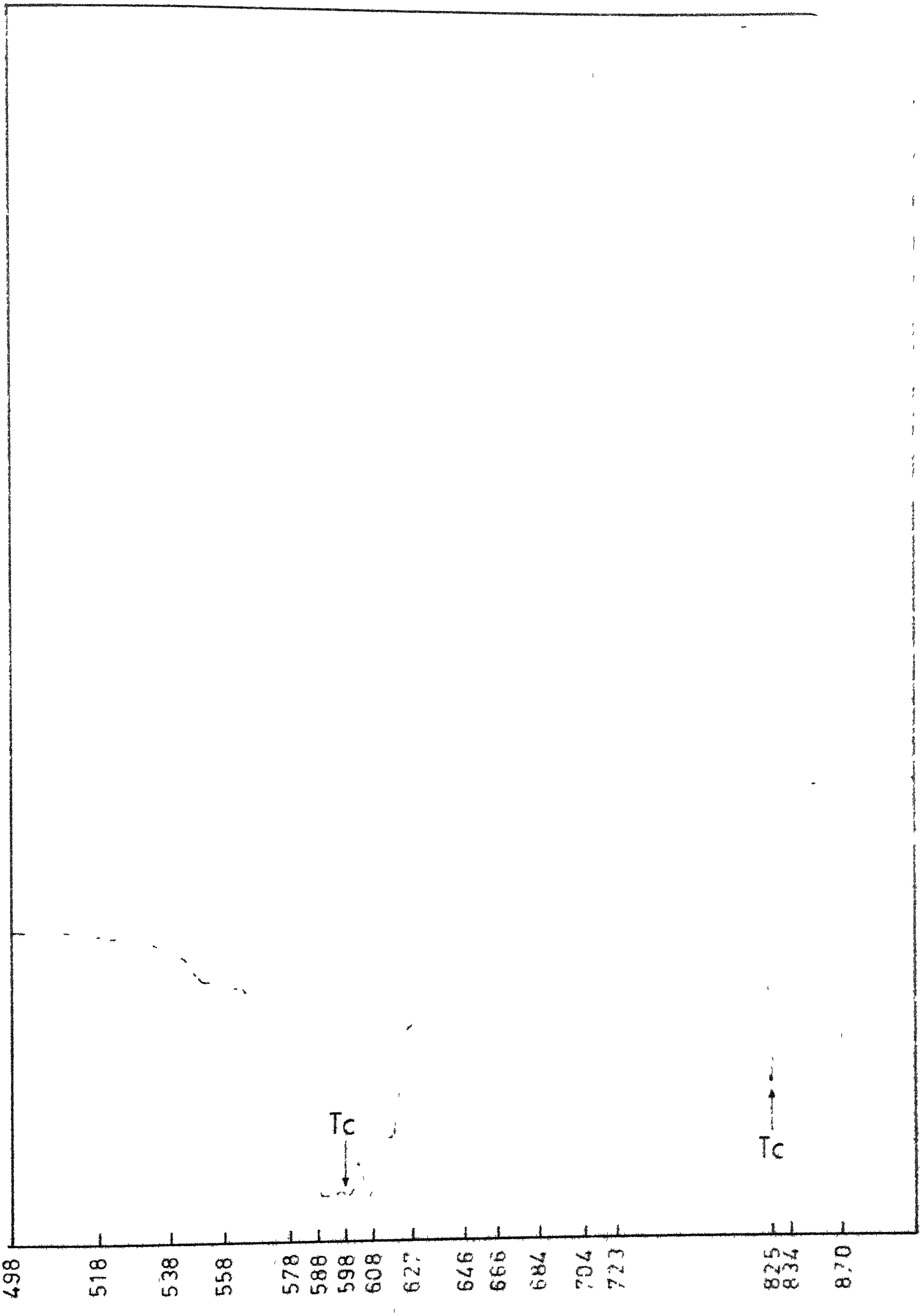

FIG.IV.16. CURIE TEMPERATURE PLOT FOR ALLOY -30 ($RE_{15}Co_{65}Fe_{20}$)

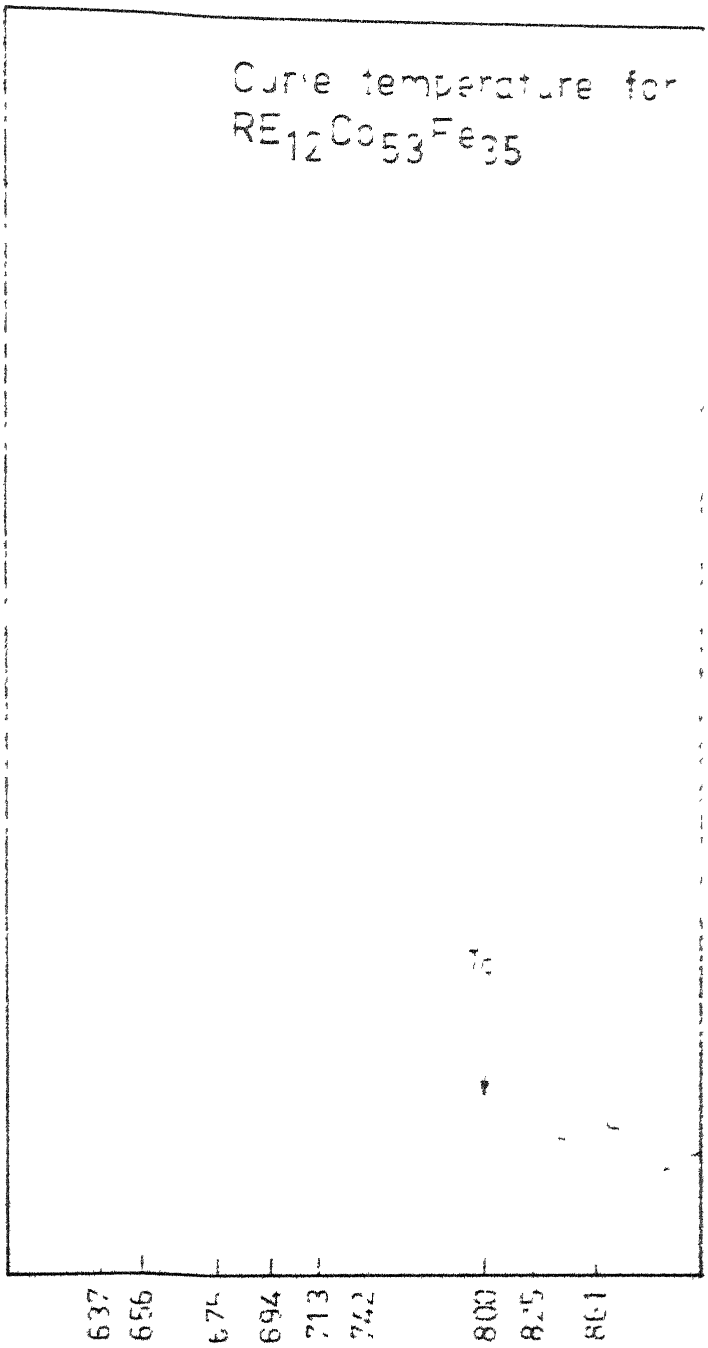

FIG. IV. 17 CURIE TEMPERATURE E

of RE_2Co_7 phase in alloy 30. In general, a small drift was observed when the same specimen was used repeatedly for Curie temperature determination. Hence, the T_c value obtained in the first or the second run was considered to be accurate. The Curie temperatures of different alloys are tabulated in Table IV.7 and the T_c values are plotted as a function of Fe content of the alloys in Fig. IV.18. As shown in the figure, the Curie temperatures of various phases appear to vary smoothly with Fe content. Among the various alloys investigated, the Curie temperatures of the A phase alloys are the lowest and those of the S phase alloys are the highest. For the S phase the Curie temperature appears to increase initially (upto about 25 at. pct.Fe) but with further additions of Fe, T_c decreases. In the case of the A phase, the Curie temperature decreases with increase in Fe, the decrease being less marked initially. For the RE_2Co_7 phase the Curie temperature increases with increase in Fe. For the binary RE-Co alloys the addition of Fe is reported to decrease the Curie temperature (see Fig. I.8). But, as shown in Fig. IV.18, the Curie temperatures remain attractively high even after substantial amounts of Fe addition in the S phase.

From the data on the Curie temperatures and the easy axis of magnetization of the RE-Co-Fe alloys, it appears that the S phase offers the maximum potential for the development of permanent magnets. If the prediction that the $RE_2(Co,Fe)_{17}$

TABLE IV.7

Curie Temperatures of RE-Co-Fe Alloys

Serial No.	Alloy No.	Major Phase	Intended Composition at.per cent Fe	Curie Temperature of the major phase T_c, °C
1	12	RE_2Co_7	15	718.0
2	14	RE_2Co_7	20	722.5
3	52	RE_2Co_7	30	732.0
4	30	S-phase	20	825.0
5	48	S-phase	25	835.0
6	51	S-phase	35	800.0
7	31	S-phase	50	700.0
8	42	A-phase	40	568.0
9	33	A-phase	46.5	552.0
10	34	A-phase	50	513.0

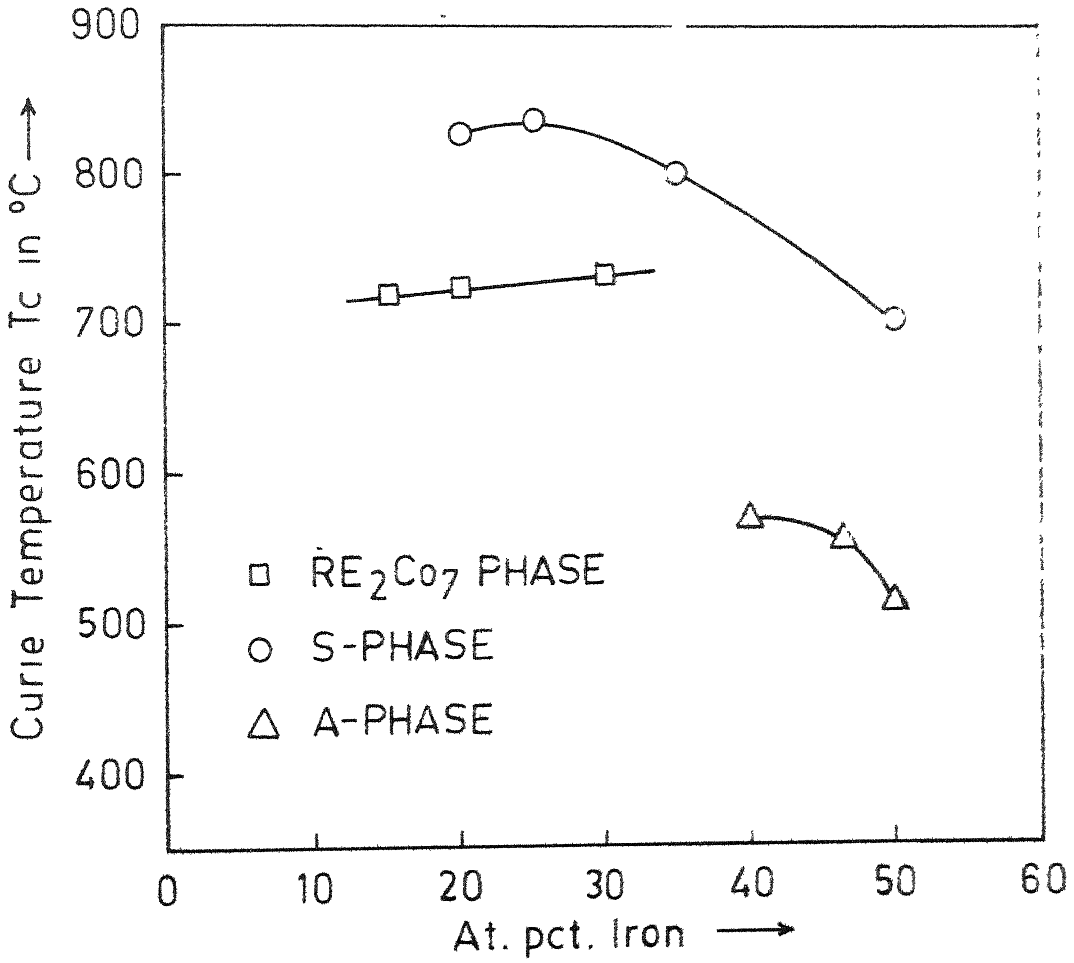

FIG. IV.18 CURIE TEMPERATURES OF RE-Co-Fe PHASES.

phase reported in literature (32) actually corresponds to the S phase is true, then very high magnetization values are also expected for the S phase. Even otherwise, since the addition of Fe is reported to increase the saturation magnetization (30), it is expected that the S phase will have higher saturation magnetization values compared to the binary $RECo_5$ alloys. Thus, the S phase is expected to have better magnetic properties compared to the $RECo_5$ type and RE_2Co_{17} type phases. Also, it offers higher economic advantages compared to the $RECo_5$ and RE_2Co_{17} compounds because it takes more of iron than the $RECo_5$ type compounds and more of mischmetal than the RE_2Co_{17} type compounds.

IV.4 Thermal Analysis:

Thermal analysis was tried with alloys which were not from the group of alloys investigated. The reason for this was that (1) due to the material used in the construction of thermal analysis apparatus, it could be used only upto 1400°C and (2) the approximate range of melting points of the investigated high Fe alloys could not be guessed. Hence, for first trial runs the alloys investigated in the present work were not suitable. Because of these reasons, two alloys with the lowest Fe content possible, 13.25 at. pct. RE, 83.8 at. pct. Co and 2.95 at. pct. Fe and 16.42 at. pct. RE, 79.92 at. pct. Co and 3.66 at. pct. Fe (57) were made use of. The usual melting points of RE-Co alloys between $RECo_5$ and

RE_2Co_{17} phases are in the range of 1200°C to 1350°C. The MM-Co alloys of similar compositions (but with no Fe) are also expected to show similar transformation temperatures. Hence, with 2 to 4 percent Fe addition (as is present in the chosen alloys) the melting points are not expected to be too far off from the binary ones. The first thermal analysis run was made with the 2.95 at. pct. Fe alloy containing $RECo_5$ and RE_2Co_{17} phases. In this trial run the thermocouple sheath was kept outside the alloy charge while the furnace was being heated. When the furnace temperature reached 1350°C the thermocouple along with the sheath was tried to be pushed into the melt. This was, however, not possible. Raising the furnace temperature to 1400°C also did not make it possible to insert the thermocouple into the melt. On cooling the furnace the alloy charge in the crucible was found to have melted because the granular material charged had become a solid mass showing that melting had occured. The possible reason why the thermocouple could not be inserted in the melted mass is the presence of large amount of solid RE_2Co_{17} phase having melting point higher than 1400°C. Molten part of the alloy is possibly the $RECo_5$ phase of lower melting point. Even though thermal analysis was not possible with RE-Co-Fe alloy one important observation made was that no reaction of the melt occured with the crucible even though the crucible was in contact with the hot alloy for more than three hours and with the molten alloy for more than 1/2 hr. A second trial run was made with a high RE alloy having all the $RECo_5$ phase. Since no reaction between the material charged and the alumina crucible was visible in the previous trial, in the second trial run the thermocouple along with the alumina sheath was inserted in the charge from the very beginning. The furnace was heated upto about 1250°C but at this point the furnace failed and the thermal analysis could not be carried out. On opening the thermal analysis apparatus it was found that a part of the furnace assembly had burnt out. The material charged was again found in the form of a solid mass. There was no reaction between the melt and the crucible or the thermocouple sheath. No further work could be carried out with this apparatus.

Even though the thermal analysis work could not be carried out with the present set up the trial runs indicated that (1) the crucibles fabricated were suitable for melting as well as carrying out thermal analysis work of the RE-Co-Fe alloys, (2) the RE_2Co_{17} phase having about 3 at. pct. Fe had considerably higher melting point than the binary RE_2Co_{17} phases and (3) the melting point of $RE(Co,Fe)_5$ alloy containing about 4 at. pct. Fe had a melting point below 1250°C. The furnace assembly in the thermal analysis apparatus worked quite well at 1000°C and even at 1400°C during calibration and the first trial run. The temperature control and control of heating and cooling rates was quite satisfactory for carrying out thermal analysis with small amount of material.

The failure of the furnace in the second trial run is not clearly understood. Failure may be caused by oxidation of Mo wire and the oxide reacting with alumina to cause fusing of the refractory mass. Purified argon gas was used for protecting the furnace element. A leak in the gas purification system and supply line is a possibility. Since no abnormality was found in the gas flow, the chance of a large leak is remote. Moreover, oxidation does not appear to be the real cause because the charge was RE alloy and RE elements being very reactive are expected to act as a getter thereby saving Mo from oxidation. The Mo wire in the sound portion of the furnace assembly also did not show any evidence of oxidation. Similarly, the RE-Co-Fe alloy charge was found to be clean and free from any oxide layer. Because of these observations, it appears that the failure of the furnace was possibly not due to oxidation. The only other possibility is the local excessive heating giving higher temperature at certain portion of the crucible and thereby melting the refractory cement used for holding the Mo winding on the [illegible] former.

6) The easy axis of magnetization of the S phase is along the c-axis.

7) The S phase, among the three phases found in this investigation, appear to offer the maximum potential for the development of permanent magnets. The S phase alloys have high Curie temperatures. The S phase also exhibits the desirable easy c-axis magnetic symmetry.

8) The thermal analysis apparatus designed can be used, after making small changes, for determining the melting points of alloys using small amounts of materials.

SUGGESTIONS

Basing on the results obtained in the present investigation, the following suggestions can be made for studies in this field:

1) The exact composition of MM can be determined in order to establish the correct composition ranges of different RE-Co-Fe phases existing in the isothermal section at 900°C.

2) Detailed structural investigations of the A and S phases can be carried out in order to explain the lattice parameter variations observed in these phases as a function of Fe content.

3) The easy axes of magnetization of the S phase alloys can be determined as a function of Fe content to ensure that the c-axis magnetic symmetry is maintained throughout the S phase region.

4) Even though the thermal analysis apparatus to be able to determine the melting points of the RE-Co-Fe alloys, a DTA apparatus is expected to give a more sensitive detection of melting points using still smaller amounts of charge. Since the present TA apparatus can be converted easily to a DTA apparatus, such a conversion seems to be worthwhile.

5) The primary magnetic properties (M_s and ${}_IH_c$) of the RE-Co-Fe alloys, particularly the S phase alloys, can be

determined in order to establish the optimum composition for developing the permanent magnets.

6) Since the S phase appears to be promising, efforts can be directed at the fabrication of magnets from the S phase alloys.

REFERENCES

1. Rare Earth Permanent Magnets, by E.A. Nesbitt and J.H. Wernick, Academic Press, N.Y. (1973)

2. G.W. Urbain, P. Weiss and F. Trombe, Compt. Rend, 200, 2132 (1935)

3. E. A. Nesbitt, J.H. Wernick and E. Corenzwit, J. Appl. Phys., 30, 365 (1959)

4. W.M. Hubbard, E. Adams and J.V. Gilfrich, J. Appl. Phys., 31, 368S (1960)

5. G. Hoffer and K.J. Strnat, IEEE Trans. Magn., Vol. MAG-2. 487 (1966)

6. D.K. Das, IEEE Trans. Magn., Vol. MAG-5, 214 (1969)

7. D.L. Martin and M.G. Benz, Int. Conf. Magnetism, Grenoble. France, Sept. (1970)

8. K.J. Strnat, IEEE Trans. Magn, Vol. MAG-8, 511 (1972)

9. Rare Earth Alloys, by K.A. Gschneidner Jr., D. Van Nostrand Comp. Inc., Princeton,N.J., U.S.A. (1961)

10. H.R. Kirchmayr, Z. Angew. Physik., 27, 18 (1969)

11. K.H.J. Buschow, Phys. Stat. Sol. (a), 7, 199 (1971)

12. A.E. Ray, Proc. 7th R.E. Res. Conf., 473 (1968)

13. K.J. Strnat, G. Hoffer and A.E. Ray, IEEE Trans. Magn., Vol. MAG-2, 489 (1966)

14. C. Herget and H.G. Domazer, Goldschmidt Informiest, 4, 3 (1975)

15. A.E. Ray, A.T. Biermann, R.S. Harmer and J.E. Davison. Cobalt, 4, 103 (1973)

16. K.H.J. Buschow and A.S. Van der Goot, J. Less. Comm. Metals. 14, 323 (1968)

17. Y. Khan, J. Less. Comm. Metals, 34, 191 (1974)

18. K.H.J. Buschow, J. Less. Comm. Metals, 29, 283 (1972)

19. A.E. Ray, Cobalt, 1, 13, (1974)

20. K.H.J. Buschow and W.A.J.J. Velge, J. Less. Comm. Metals, 13, 11 (1967)

21. J.H. Wernick and S. Geller, Acta. Cryst., 12, 662 (1959)

22. Y. Khan, Z. Metallkd., 65, 489 (1974)

23. K. Nassau, L.V. Cherry and W.E. Wallace, J. Phys. Chem. Solids, 16, 131 (1960)

24. E.A. Nesbitt, H.J. Williams, J.H. Wernick and R.C. Sherwood, J. Appl. Phys., 33, 1674 (1962)

25. R. Lemaire, R. Pauthenet and J. Schweizer, IEEE Trans. Magn., Vol. MAG-6, 153 (1970)

26. K.S.V.L. Narasimhan, W.E. Wallace, R.D. Hutchens and J.E. Greedan, AIP Conf. Proc. No. 18, 1212 (1974)

27. A.E. Ray and K.J. Strnat, IEEE Trans. Magn., Vol. MAG-8, 516 (1972)

28. C.W. Allen, D.L. Kurozar and A.E. Miller, IEEE Trans. Magn., Vol. MAG-10, 716 (1974)

29. E.A. Nesbitt, J. Appl. Phys., 40, 1259 (1969)

30. K.H.J. Buschow, J. Less. Comm. Metals, 31, 359 (1973)

31. A.E. Ray et al., AIP Conf. Proc. No. 10, 613 (1973)

32. K.J. Strnat and A.E. Ray, Goldschmidt Informiest, 4, 47 (1975)

33. C.C. Koch, J. Less. Comm. Metals, 22, 149 (1970)

34. S.G. Fishman and C.R. Krowe, J. Less. Comm. Metals, 29, 253 (1972)

35. K.J. Strnat, J.C. Olson and G. Hoffer, J. Appl. Phys. 39, 1263 (1968)

36. M. Mc Caig, IEEE Trans. Magn., Vol. MAG-6, 198 (1970)

37. C.J. Fellows and R.E. Johnson, Cobalt, 56, 141 (1972)

38. D.K. Das, AIP Conf. Proc. No. 10, 628 (1973)

39. H. Nagel and A. Menth, Goldschmidt Informiest, 4, 42(1975)

40. D.L. Martin, J.T. Geertsen, R.P. Laforce and A.C. Rockwood Proc. 11th RE. Res. Conf., 342 (1974)

41. K.J. Strnat, A.E. Ray and C. Herget, Suppl. J. de Physique, 32, C1-552 (1971)

42. S. Takata, Nippon Kinzoku Gakkai-Si, 37, 222(1973)

43. E.A. Nesbitt, G.Y. Chin, R.C. Sherwood, M.L. Green and H.J. Leany, IEEE Trans. Magn, Vol. MAG-9, Sept. (1973)

44. Rare Earth Permanent Magnets, by E.A. Nesbitt and J.H. Wernick, Academic Press, N.Y. (1973)

45. , J. Phys. Soc. Japan, 17, Suppl. B1, 143 (1962)

46. D.L. Martin and M.G. Benz, AIP Conf. Proc. No. 5, 970 (1972)

47. R.E. Cech, J. Appl. Phys., 41, 5247 (1970)

48. D.K. Das, IEEE Trans. Magn., Vol MAG-7, 432 (1971)

49. S. Chander, B.Tech, thesis, I.I.T., Kanpur (1968)

50. A.E. Ray and K.J. Strnat, Technical Report AFML-TR-71-53, Wright Patterson Air Force Base, Ohio (1971)

51. J.L. Haughton and M.L. Becker, J. Iron. Steel Inst. 121, 315 (1930)

52. T. Murakami, Sc. Rep. Tohoku Imp. Univ., 10, 79 (1921); 16, 481 (1927)

53. G. Fhragmen, J. Iron. Steel. Inst., 114, 397 (1926)

54. A. Osawa and T. Muraka, Nippon Kinzoku Gakkai-Si, 4, 22 8 (1940)

55. Constitution of Binary Alloys, by M. Hansen and K. Anderko, McGraw-Hill Book Comp. N.Y. (1958).

56. Y. Khan, Acta. Cryst., B 29, 2502 (1973)

57. R.C. Mittal, M.Tech. Thesis to be submitted shortly.

58. K.N.R. Taylor and C.A. Poldy, J. Less. Comm. Metals, 27, 255 (1972)

59. A.E. Ray and R.S. Harmer, Proc. 9th RE. Res. Conf., 368 (197

60. D. Givord, F. Givord, R. Lemaire, W.J. James and J.S. Shah, J. Less. Comm. Metals, 29, 389 (1972).

61. V.V. Sergeyev, Personal Communication to A.E. Ray, Nov.(197

62. D. Givord, R. Lemaire, J.M. Moreau and E. Roudaut, J. Less Comm. Metals, 29, 361 (1972).

APPENDIX I

Voltage-Current-Temperature Characteristics of the Mo-wound Furnace

Room Temperature Resistance 3.0 ohms.

Voltage volts	Current amps.	Temperature °C
5	1.6	150
10	2.15	280
15	2.65	410
20	3.15	535
25	3.6	640
30	3.9	735
35	4.2	815
40	4.45	890
45	4.7	960
50	4.85	1035
55	5.1	1100
60	5.3	1150
65	5.5	1200
70	5.7	1245
75	5.85	1285
80	6.0	1330
85	6.15	1370

A 51349

Date Slip 51349

This book is to be returned on the date last stamped.

CD 6 72 9

MSP-1977-M-SAT-PHA.